HHS Public Access

Author manuscript

Autism Res. Author manuscript; available in PMC 2018 January 01.

Published in final edited form as:

Autism Res. 2017 January ; 10(1): 42–65. doi:10.1002/aur.1664.

Novel Shank3 Mutant Exhibits Behaviors With Face Validity for Autism and Altered Striatal and Hippocampal Function

Thomas C. Jaramillo[†], **Haley E. Speed**[†], **Zhong Xuan**, **Jeremy M. Reimers**, **Christine Ochoa Escamilla**, **Travis P. Weaver**, **Shunan Liu**, **Irina Filonova**, and **Craig M. Powell**

Department of Neurology and Neurotherapeutics, University of Texas Southwestern Medical Center, Dallas, Texas (T.C.J., H.E.S., Z.X., J.M.R., C.O.E., T.P.W., S.L., I.F., C.M.P.); Department of Psychiatry and Neuroscience Graduate Program, University of Texas Southwestern Medical Center, Dallas, Texas (C.M.P.)

Abstract

Mutations/deletions in the *SHANK3* gene are associated with autism spectrum disorders and intellectual disability. Here, we present electrophysiological and behavioral consequences in novel heterozygous and homozygous mice with a transcriptional stop cassette inserted upstream of the PDZ domain-coding exons in *Shank3* (Shank3^{E13}). Insertion of a transcriptional stop cassette prior to exon 13 leads to loss of the two higher molecular weight isoforms of Shank3. Behaviorally, both Shank3^{E13} heterozygous (HET) and homozygous knockout (KO) mice display increased repetitive grooming, deficits in social interaction tasks, and decreased rearing. Shank3^{E13} KO mice also display deficits in spatial memory in the Morris water maze task. Baseline hippocampal synaptic transmission and short-term plasticity are preserved in Shank3^{E13} HET and KO mice, while both HET and KO mice exhibit impaired hippocampal long-term plasticity. Additionally, Shank3^{E13} HET and KO mice display impaired striatal glutamatergic synaptic transmission. These results demonstrate for the first time in this novel *Shank3* mutant that both homozygous and heterozygous mutation of *Shank3* lead to behavioral abnormalities with face validity for autism along with widespread synaptic dysfunction.

Keywords

autism spectrum disorder; Shank3; Phelan-McDermid syndrome; mouse model; social interaction; grooming

Introduction

Shank3 is a multidomain protein in the postsynaptic density (PSD) of excitatory synapses [Boeckers et al., 2002; Naisbitt et al., 1999]. It contains functional and diverse binding motifs such as an ankyrin repeat, SH3, prolinerich, PDZ, and SAM domains. Through its PDZ domain, Shank3 interacts with GKAP/PSD-95/glutamate receptor complexes [Ehlers,

Address for correspondence and reprints: Craig M. Powell, craig.powell@utsouthwestern.edu.

[†]T.C.J. and H.E.S. contributed equally to this work.

Author contributions: T.C.J., H.E.S., J.M.R., and C.M.P. designed research; T.C.J., H.E.S., Z.X., J.M.R., C.F.O., S.L., and I.F. performed research; T.C.J., H.E.S., and J.M.R. analyzed data; T.C.J., H.E.S., J.M.R., and C.M.P wrote the paper.

1999; Naisbitt et al., 1999], and through its Homer binding domain, it binds to the Homer-group1 metabotropic glutamate receptor (mGluR1) complex [Tu et al., 1999]. Through these interactions Shank3 aids in assembly of signaling complexes at the synapse to govern spine development, protein targeting, and signal transduction [Arons et al., 2012; Duffney et al., 2013; Ehlers, 1999, 2002; Park et al., 2003; Roussignol et al., 2005; Verpelli et al., 2011].

Genetic alteration of the *SHANK3* gene is associated with neuropsychiatric disorders [Bonaglia et al., 2001; Durand et al., 2007; Gong, Lippa, Zhu, Lin, & Rosso, 2009; Gauthier et al., 2010; Grabrucker et al., 2014; Misceo et al., 2011; Moessner et al., 2007; Vucurovic et al., 2012]. Heterozygous deletion of *SHANK3* is causative in the 22q13 deletion syndrome (Phelan-McDermid syndrome, PMS), characterized by hypotonia, social withdrawal, delayed psychomotor development, repetitive behaviors, and mild dysmorphic features [Kolevzon et al., 2011; Sarasua et al., 2011; Soorya et al., 2013]. Approximately 75% of PMS patients meet autism diagnostic criteria [Soorya et al., 2013]. Mutations/deletions of *SHANK3* are also associated with autism spectrum disorders (ASD) and schizophrenia [Bozdagi et al., 2010; Gauthier et al., 2010; Grabrucker et al., 2014; Guilmatre et al., 2014; Herbert, 2011].

Tremendous phenotypic heterogeneity exists in patients with alterations in *SHANK3*, which can pose challenges to diagnosis and treatment. One potential contributor is the extensive array of *SHANK3* isoforms. ASD-associated *SHANK3* alterations can disrupt isoform expression or domain structure and function in the various isoforms. Typically, studies involving Shank3 protein expression focus on three major isoforms (α β γ) [Han et al., 2013; Peca et al., 2011; Wang et al., 2011]. Additional studies, however, reveal that the *Shank3* gene has multiple promoters and is alternatively spliced, suggesting that the number of Shank3 isoforms can be extensive [Kouser et al., 2013; Speed et al., 2015; Wang et al., 2011; Wang, Xu, Bey, Lee, & Jiang, 2014].

To further evaluate Shank3 isoform-specific phenotypes we generated a *Shank3* mutant mouse targeting disruption of the PDZ domain with a transcriptional stop cassette prior to exon 13, leading to loss of the two higher molecular weight isoforms. These Shank3^{E13} heterozygous (HET) and homozygous (KO) mutants display phenotypes with face validity for autism such as increased repetitive grooming and deficits in social interaction. Shank3^{E13} KO mice also display spatial memory deficits while HET and KO mice display impaired hippocampal LTP and striatal glutamatergic synaptic transmission.

Materials and Methods

Shank3^{E13} Mutant Mice

The construct inserted a neo-stop cassette into a unique Bgl II site in intron 12 of the *Shank3* gene [Dragatsis & Zeitlin, 2001; Guy, Selfridge, Cobb, & Bird, 2007]. The neo-Stop cassette was flanked by loxP sites. Targeting vector was pBluescript II SK (±) (Agilent). The final construct had a 5′ homology (1042 bp) and a 3′ homology (5823 bp) arm with a 3020 bp DNA fragment containing floxed neo-stop cassette inserted. A DT (diphtheria toxin) cassette was included for negative selection. The linearized construct (by Sal1) was electroporated into embryonic stem (ES) cells (129s6SvEvTac) and clones were selected for G418

resistance. The correctly targeted ES clones were identified by PCR using three primers (Forward: screen-13E-s-1 **CATGGTAAGTGACTCCAG TTTTTGCTCAGATAC**, Reverse (1): screen-13E-s-2-1 **GAATTCGATGACCTCGAGGATCTATAACTTCG**, Reverse (2): screen-13E-s-3 **CAACTTAAAGTCGAG GTTGACAGA GGTTACCAC**); WT5921 bp band, KI (knock-in)51267 bp band. Correct targeting was confirmed by sequencing PCR products, and genomic DNA was analyzed by Southern blot. Positive ES clones were injected into blastocysts (C57BL6J) generating chimeras at the UT Southwestern Transgenic Facility. Chimeras were bred with C57BL/6J to confirm germline transmission identified by PCR with three primers: Forward (1): loxp1-sequence **CCATGCGTCAAACTTGATGGATGCCTAG**, Forward (2): 24M–up-loxp2–501 **CTTACTCCACACAGGCATAGAGTGTCTG**, Reverse: 13E-Gtyping-antisense-1 **GAGCACTAACTGCTCTTCTGAAGGTC**; WT DNA = 332 bp band, KI DNA = 576 bp band. The KI mice ($Shank3^{E13}$) were backcrossed with C57BL/6J for at least four generations.

Other Shank3 Mutant Mice

Previously we generated and characterized three other Shank3 mutant mice e4–9 [Jaramillo et al., 2016] and G/G [Speed et al., 2015], ΔC/ΔC [Kouser et al., 2013]. The ΔC/ΔC Shank3 mice were a collaborative gift from Dr. Paul Worley. These mice were all used in this study to compare exon presence using Southern blot analysis in Figure 1.

Western Blot

Synaptosome and whole cell lysate and preparation—Synaptosomes and whole cell lysates were prepared as previously described [Kouser et al., 2013].

Western blot and antibodies—For Western blotting, samples were diluted in 2 × Laemmli sample buffer containing 2-mercaptoethanol (Bio-Rad, Hercules, CA, USA) and boiled for 10 min. Five to twenty microgram of protein were loaded and blotted with antibodies specific for synaptic proteins: anti-GluR1 (Abcam, Cambridge, England), anti-GluR2 (Invitrogen, Carlsbad, CA, USA), anti-GluR3 (Cell Signaling, Danvers, MA, USA), anti-NR1 (Sigma, St. Louis, MO, USA), anti-NR2A (Sigma, St. Louis, MO, USA), anti-NR2B (NeuroMAB, Davis, CA, USA), anti-Shank3 C-terminal (gift from P Worley; raised against residues 1379–1740 and 1379–1675), anti-mGluR5 (Millipore, Billerica, MA, USA), anti-PSD-95 (Calbiochem, Billerica, MA, USA), anti-Homer 1 b/c (Santa Cruz, Santa Cruz, CA, USA). Anti-β-Actin (Sigma, St. Louis, MO, USA) was used as loading control. Blots were incubated with HRP-conjugated anti-rabbit, anti-mouse secondary antibodies (GE Healthcare, Dallas, TX, USA). For some samples, we used clarity western ECL (Bio-Rad, Hercules, CA, USA), and exposed film was developed by an Image Works film processor. We also used fluorescent secondary IRDye® anti-Rabbit (product #: 926–32212) or anti-mouse (product #: 926–68071) at 1:10,000 (LI-COR) for some. Fluorescence was visualized with Odyssey fc® . Signals were quantified using Image Studio (LiCor, Lincoln, Nebraska, USA), normalized to β–actin, and analyzed using Microsoft Excel (Redmond, WA) and Graphpad Prism (La Jolla, CA).

Behavioral overview

All mice were age- and sex-matched, littermate progeny of heterozygous Shank3^{E13} mutants. Behaviors were performed by experimenters blind to genotypes. The behavioral cohort consisted of 55 mice; n = 20 wildtype (WT, ten female and ten male), n = 15 heterozygous (HET, seven male and eight female), n = 20 homozygous (HOMO, ten female and ten male), that were 5.4– 9 weeks of age to start. Thus, we tested seven male littermate trios (WT/het/homo), eight female littermate trios (WT/het/homo), three male littermate pairs (WT/homo), and two female littermate pairs (WT/homo). Behaviors were tested in the following order: elevated plus maze, dark/light, open field, locomotor, rearing, grooming, 3-box social interaction, caged conspecific (social interaction with a caged adult), rotarod, juvenile social interaction, genotype/sex-matched adult social interaction, marble burying, Morris water maze, prepulse inhibition of startle, and startle threshold. Results are presented in different order than tested to ease the flow of presentation. Analysis used StatPlus software (Version 2015, AnalystSoft, Alexandria, VA, USA) using either two-way ANOVAs or three-way repeated measures ANOVA with genotype and sex as the main variables and appropriate repeated measure. Post-hoc planned comparisons were applied for significant effects and interactions. For detailed statistical results see Table 1.

Behavioral tests

Elevated plus maze—was conducted as described previously [Etherton, Blaiss, Powell, & Sudhof, 2009]. Briefly, mice were placed in the center of the maze (each arm was 30 cm long and 5 cm wide with 25 cm high walls on the closed arms) and allowed to freely explore for 5 min. All mice were tested under dim white light at ~7 lux. Noldus Ethovision version 3.1 (Leesburg, VA, USA) was used to track and record mouse behavior.

Locomotor and Rearing activity—was measured as described previously [Etherton et al., 2009; Powell et al., 2004; Tabuchi et al., 2007]. Mice were placed in novel cages (a clean cage with the same dimensions as their home cage; L × W × H = 27.3 × 16.5 × 12.7 cm^3) with minimal bedding and allowed to freely explore for 2hr under red lighting. Horizontal locomotor activity (i.e. the number of photobeam breaks) was measured by computer software (San Diego Instruments; San Diego, CA, USA), and data were analyzed in 5-min bins.

Rearing activity—was measured in the same manner as locomotor activity, however recording only occurred over a 1-hr time period. Additionally, the photobeams were raised to 3 cm higher to detect rearing of the mouse but not locomotor activity.

Dark/Light test—was conducted as described previously [Blundell et al., 2009; Powell et al., 2004]. Mice were placed in the dark chamber (each chamber was 25 × 26 cm with 2066 lux on the light side and ~1 lux on the dark side) and allowed to habituate for 2 min. After habituation, mice were allowed to freely explore both chambers for 10 min.

Rotarod—was conducted as described previously [Powell et al., 2004]. Briefly, mice were placed on a stationary rotarod (IITC Life Science) that was then activated and accelerated from 0 to 45 revolutions/min over 5 min. The latency for the mice to fall off the rod was

measured. If a mouse held onto the rotating rod for one complete revolution it was scored as a fall. Each mouse received four trials per day for 2 days. Within a day, each trial had an intertrial interval of ~45 min.

Open Field—was conducted as described previously [Etherton et al., 2009]. Briefly, mice were placed along the edge of an open arena (44×44×44 cm, ~7 lux) and allowed to freely explore for 10 min. Time spent in the center of the arena (15 × 15 cm) as well as locomotor activity were measured. Mice were monitored using CleverSys TopScan Software (Reston VA).

Social interaction with a novel juvenile target mouse—was performed essentially as described [Blundell et al., 2009; Kwon et al., 2006; Tabuchi et al., 2007]. Briefly, following a 15-min habituation under red light, the experimental and target mice were placed in a novel cage for 2 min and allowed to directly interact with a novel C57BL6J juvenile mouse (3 weeks of age; Jackson labs). Interaction was scored by observing the duration and number of times the test mouse initiated contact with or sniffed the juvenile mouse. Contact was considered as any part of the body touching the other mouse. Three days later the same experimental and novel juvenile mice were paired again in a novel cage for 2 min and scored in the same manner.

Social interaction with a caged adult—was performed as described [Blundell et al., 2010a]. Briefly, the test was performed in a 48 × 48 cm^2 white plastic arena under red light using $3.5'' \times 30'' \times 2''$ (w × h × l) clear rectangular cage containing a novel adult mouse. The lower half of the rectangular cage has small openings to allow for olfactory and minimal tactile interaction. Initially mice were allowed to explore the arena for 5 min with an empty rectangular cage. Then, mice were allowed to approach a novel adult mouse housed in the rectangular cage for another 5 min.

Social interaction with genotype- and sex-matched pairs—was performed by pairing mice with a sex- and genotype-matched partner within the experimental cohort. Matched pairs were derived from separate cages and were never previously housed together. Mouse pairs were placed at separate ends in an open field arena (44 × 44 × 44 cm) and allowed to interact for 5 min under dim lighting (~7 lux).

Three-chamber social approach—social preference and social novelty was tested using a three-chambered box as described previously [Blundell et al., 2009] and based to a large extent on the original descriptions [Moy et al., 2004; Nadler et al., 2004]. This test consisted of three 10-min trials. During the first trial, the mouse was allowed to explore the 3 chamber box in which each end-chamber contained an empty cage (upside down pencil holder). In the second trial, the 3-chamber box contained a novel stimulus mouse under a cage in one of the end-chambers and an empty cage in the opposite end-chamber. The test mouse was free to choose between an inanimate cage and a caged, social target. For the third trial, the test mouse was free to choose between a caged novel social target (novel mouse) versus the same caged mouse in trial 2 (familiar social target). Locations of empty cages and social targets were counterbalanced, and mice were placed back into the home cage for very brief intervals

between trials. Social interactions/approaches were objectively monitored and scored using video-tracking and automated CleverSys Social Scan Software (Reston VA).

Grooming—as performed by placing mice into an empty cage and monitoring and video recording for 10 min. Time spent grooming the face, head, body, or tail, are all considered grooming.

Morris water maze—was conducted as previously described [Powell et al., 2004]. Briefly, in a 120 cm diameter pool a 10-cm diameter circular platform was submerged ~1 cm below the surface of the water (22 ± 1 °C) made opaque with white, nontoxic tempra paint. After finding the platform or being guided by the experimenter to the platform if the 60-sec trial elapsed, mice remained on the platform for 15 sec before being removed and returned to their home cage. Training was conducted over 7 consecutive days, followed by a probe trail on day 8 (60-sec swim with no platform). To test basic visual function, we measured the latency to reach the platform with a visible cue atop the platform in the water maze on day 14.

Prepulse inhibition and startle: Both prepulse inhibition and startle response were conducted as previously described [Blundell, Kaeser, Sudhof, & Powell, 2010b]. Briefly, mice were placed inside a cylinder mounted atop a piezoelectric accelerometer that detected and transduced animal movements inside the startle chambers (San Diego Instruments, San Diego, CA, USA). Acoustic stimuli varying in decibels (dB) were delivered by high-frequency speakers mounted 33 cm above the cylinder. To test startle response mice were exposed to stimuli ranging from 0 to 120 db and the amplitude of the startle responses was obtained in arbitrary units. For prepulse inhibition (PPI), mice were subjected to five trial types in a 22-min session: pulse alone (40 msec, 120 dB, white noise pulse), three different prepulse/pulse trials (20 msec prepulse of 4, 8, or 16 dB above background noise level of 70 dB preceded the 120 dB pulse by 100 msec onset-onset interval), and no stimulus. All trials were presented pseudorandomly with an average of 15 sec (7–23 sec) between the 62 trials. Prior to testing, mice were acclimated to the cylinders for 5 min then tested in four blocks of test trials. The first and last blocks consisted of six pulse-alone trials. Blocks 2 and 3 each contained six pulse-alone trials, five of each level of prepulse/pulse trials, and five no-stimulus trials.

Marble burying: As described previously [Blundell et al., 2010a], individual mice were placed in a novel home cage with 5 cm of bedding. Twenty marbles were evenly placed on top of the bedding throughout the home cage, and mice were free to explore the cage for 30 min. After 30 min the number of marbles buried was recorded. A marble was defined as buried when <25% of the marble was visible. This test was conducted in a well-lit room (~80 lux).

Physiology

Acute slice preparation: Four to six week old male mice were anaesthetized with 8% chloral hydrate (400 mg/kg) and transcardially perfused with artificial cerebral spinal fluid (ACSF) containing (in mM): 120 NaCl, 3.5 KCl, 1.25 NaH_2PO_4, 1 $MgSO_4$, 26 $NaHCO_3$, 10

dextrose, and 2 $CaCl_2$ adjusted to pH 7.4 and saturated with 95% O_2/5% CO_2. Brains were rapidly removed and placed in ice-cold sucrose ACSF containing (in mM): 75 sucrose, 87 NaCl, 3 KCl, 1.25 NaH_2PO_4, 7 $MgSO_4$, 26 $NaHCO_3$, 20 dextrose, and 0.5 $CaCl_2$ adjusted to pH 7.4 and saturated with 95% O_2/5% CO_2. Coronal slices containing dorsal hippocampus or thalamocortical slices containing dorsal striatum (300–400 μm) were made using VT1000s Vibratome (Leica Biosystems, Buffalo Grove, IL, USA). Slices recovered at 35°C for 30–45 min in ACSF and slowly cooled to room temperature before recording.

Extracellular "field" recordings—were performed as previously described [Kouser et al., 2013; Speed et al., 2015]

Whole-cell patch clamp recordings: Excitatory postsynaptic currents were recorded from cell bodies identified at 80 × on an AxioExaminer D1 Differential Interference Contrast (DIC) microscope (Zeiss, Thornwood, New York, USA). CA1 neurons were identified by triangular appearance and large apical dendrite. Striatal medium spiny neurons (MSNs) were identified by their oval shape, multiple dendrites, and hyperpolarized resting membrane potential (approximately −85mV) measured after break-in. Stimulating electrode was placed just below the corpus callosum (Fig. 10A) ~150–200μm from the recorded MSN as described [Jaramillo et al., 2016]. Borosilicate glass electrodes (4–6MX) were filled with internal solution containing (in mM): 110 CsMethanesulfonate, 15 CsCl, 8 NaCl, 10 TEA-Cl, 2 EGTA, 10 HEPES, 3 QX 314, 2 ATP, 0.3 GTP. Observed junction potential was ~10 mV and was compensated. Cells with > 25% change in access resistance (15–25 MΩ) or holding current were not included. Stimulation was controlled via a Model 2200 stimulus isolator (A-M Systems, Sequim, WA, USA) though a monopolar tungsten microelectrode (FHC, Bowdoin, ME) with a 0.1 msec biphasic pulse. 100 μM picrotoxin was in bath for all experiments. Sample size (*n*) indicates number of cells with no more than five cells per mouse and five or more mice per genotype.

Data collection and analysis: All recordings were in shallow submersion chambers perfused with oxygenated ACSF at 32 ± 0.5 °C with a flow rate of 3–5 mL/min. Data were sampled at 10 kHz using Digidata 1440 digitizers with Clampex 10.3 and filtered at 1–5 kHz with either Model 1800 amplifiers (A-M Systems, Sequim, WA, USA) for field recordings or Mutliclamp 700B amplifiers (Molecular Devices, Sunnyvale, CA, USA). Raw traces were analyzed using Clampfit 10.3 (Molecular Devices, Sunnyvale, CA, USA). Statistical analysis and graphing were performed in GraphPad 6 (GraphPad Software, San Diego, CA, USA). For statistical analysis, we used genotype and sex as main factors for ANOVA analysis. In most cases, there was not a significant main effect of sex. In those cases, where there was a main effect of sex, most did not demonstrate an interaction between sex and genotype. Thus, in our figures we have combined males and females into single graphs. For those tasks where we identified an interaction between sex and genotype, we have provided average values and standard error of the mean in our statistical table as well as separate figures of the male and female data for those most interested in sex differences. We never "combined" our male and female data in our statistical analyses, rather maintaining sex as an independent variable as is appropriate for ANOVA statistics.

Compounds and drugs: Octahydro-12-(hydroxymethyl)-2-imino-5,9:7,10a-dimethano-10aH[1,3]dioxocino[6,5-d] py rimidine-4,7,10,11,12-pentolTetrodotoxin (TTX, Tetrodotoxin), picrotoxin, *N*-(2,6-Dimethylphenylcarbamoylmethyl)triethylammonium chloride (QX 314), (R,S)-3,5-Di hydroxyphenylglycine (DHPG), CsMethanesulfonate, and CsCl were obtained from Sigma-Aldrich (Minneapolis, MN). All other reagents were obtained from Fisher Scientific (Waltham, MA).

Results

Generation of Shank3^{E13} Mice

We disrupted the *Shank3* gene in mice by insertion of a transcriptional neo-stop cassette between exon 12 (E12) and exon 13 (E13) (Fig. 1A). To ensure proper incorporation of the neo-stop cassette, we used PCR primers spanning the loxP sites (Fig. 1B). To verify correct targeting, we performed RT-PCR on brain cDNA of 4-week old Shank3^{e13} mice. Loss expression of mRNA containing exons 13–19 in Shank3^{e13} mice demonstrated correct targeting (Fig. 1C). We also show correct targeting in the Shank3$^{e4–9}$ [Jaramillo et al., 2015], an autism-associated insertion mutation in exon 21 in G/G mice [Speed et al., 2015], and *Shank3* exon 21 deletion mice (ΔC/ΔC) [Kouser et al., 2013] (Fig. 1C). Western blots of whole brain lysate using C-terminal Shank3 antibody (gift from Paul Worley) showed loss of the higher molecular weight bands in the KO mice (Fig. 1D, KO). The same antibody on whole brain lysate from a complete Shank3 KO (gift from Yong-hui Jiang) showed loss of the same bands (not shown) indicating that these bands are representative of Shank3. Remaining bands in the “KO” lane in Figure 1D were also absent from the complete Shank3 knockout, demonstrating these bands represent remaining isoforms of Shank3.

Shank3^{E13} HET and KO Mice Display Social Interaction Deficits

Because social differences are a core feature of autism and prominent features of PMS, we tested Shank3^{E13} mutant mice in a number of social tasks. In the 3-chamber test of sociability, Shank3^{E13} HET and KO mice displayed abnormalities. None of the groups displayed an initial bias for either side chamber (Fig. 2A). When one chamber contained a novel caged adult mouse and the other contained an empty cage, only WT and KO mice displayed a social preference. Shank3^{E13} HET mice did not display significant sociability (Social vs. Inanimate—WT: $P<0.005$; HET: $P=0.532$, KO: $P<0.003$; Fig. 2B). When one chamber contained a familiar caged adult mouse and the other contained a novel caged adult mouse, only WT mice showed social novelty preference. Shank3^{E13} HET and KO showed no social novelty preference (Novel vs. Familiar WT: $P<0.016$, HET: $P=0.532$, KO: $P=0.352$; Fig. 2C).

We also examined approach behavior of Shank3^{E13} mutants in an open field arena in the presence of a novel, caged adult target mouse. Shank3^{E13} KO mice displayed decreased approach of the caged adult mouse when compared to WT and HET (Social: WT vs. KO: $P<0.007$; HET vs. KO: $P<0.011$; Fig. 2D).

We also assessed reciprocal social interaction by pairing mice of the same genotype/sex for an initial encounter. Shank3^{E13} KO pairs displayed decreased social interaction compared to

WT/WT and HET/HET pairs (total interaction: WT vs. KO: P<0.0059; HET vs. KO: *P*<0.0037; **2E**). Furthermore, Shank3^{E13} KO mice displayed decreased number of social interaction bouts (WT vs. KO: *P*<2.09E-8; HET vs. KO: *P*<0.0004; Fig. 2F).

We next tested Shank3^{E13} mutants in a social recognition memory task in which novel juvenile mice (3 wk old) were introduced to experimental mice, and then 3 days later the same juvenile mice were reintroduced to the same experimental mouse. WT mice displayed a significant decrease in interaction time when the juvenile mouse was reintroduced, suggesting that WT mice recognized the juvenile as familiar. HET and KO Shank3^{E13} mice displayed a lack of social recognition memory (Initial vs. recognition time—WT: *P*<0.0005, HET: *P* = 0.901, KO: *P*=0.974; Fig. 2G).

Shank3E13 HET and KO Mice Display Increased Repetitive Grooming

Because restricted and repetitive behaviors are a core feature of autism and PMS, we monitored repetitive grooming behavior in Shank3^{E13} mutants over a 10-min period. Both HET and KO mice displayed increased time spent grooming compared to WT (WT vs. HET: *P* <0.0008; WT vs. KO: *P*<1.21E-8; Fig. 3A).

Anxiety-Like Behavior in Shank3E13 Mutants

The social and grooming differences in Shank3^{E13} mice are not explained by a more generalized anxiety-like state. In the open field (OF), all three groups spent similar time in the central, anxiogenic region (Fig. 3B). Additionally, there was no difference in total distance traveled (Fig. 3C). In the dark/light test, all groups displayed a similar latency to enter the anxiety-provoking, light chamber (Fig. 3D). All spent similar time in the light and dark chambers (Fig. 3E), although Shank3^{E13} HETs displayed a trend toward reduced time in the light chamber (Het vs. WT: *P* = 0.057; Fig. 3E). Similarly, WT and KO mice displayed similar time in open and closed arms of the elevated plus maze (Fig. 3F). HET mice, however, displayed decreased time in the open arms compared to WT (WT VS HET: *P*>0.026; WT vs. KO: *P* = 0.093; Fig. 3F).

Rearing activity in mice is thought to be a form of exploratory activity possibly linked to anxiety. Both Shank3^{E13} HET and KO mice displayed reduced rearing over successive 5-min bins during a 1-hr testing period compared to WT (WT vs. HET: *P*<0.00002; WT vs. KO: *P* < 4.21E-13; Fig. 3G). Further analysis of the cohort showed a significant sex difference with HET and KO mice displaying a significant decrease in rearing compared to female WT mice (WT vs. HET: *P*<0.04, WT vs. KO: *P* < 0.01; Fig. 3H). Male mutant mice displayed a trend of decrease rearing however it was not significant (Fig. 3I). Correspondingly, total rearing activity was significantly decreased in the Shank3^{E13} KO but not HET mice (WT vs. KO: *P*<0.016; WT vs. HET: *P*=0.201; Female: WT vs. KO: *P* < 0.023; WT vs. HET: *P*=0.105; Fig. 3J).

Lastly, we tested mice using a marble-burying task, results of which are ascribed to behavioral domains including neophobia, anxiety, or repetitive behavior. Shank3^{E13} KO mice displayed a decrease in number of marbles buried compared to WT and HET mice (WT vs. KO: *P*<3.5E–7; HET vs. KO: *P*<0.00037; Fig. 3K).

Motor Skills and Auditory Responses in Shank3E13 Mutants

Because incoordination and gait abnormalities are present in some children with autism [Shetreat-Klein, Shinnar, & Rapin, 2014] and many children with PMS [Soorya et al., 2013], we tested locomotor activity and coordination in Shank3^{E13} mutants. All groups displayed similar habituation in activity over a 2-hr period (3-way ANOVA: genotype × bin interaction P=0.550, Fig. 3L). Additionally all displayed similar total beam breaks (Fig. 3M).

To assess for coordination and motor learning deficits, we used the accelerating rotarod. Shank3^{E13} KOs displayed decreased latency to fall from the rotarod over a two-day, 8-trial period compared to WT and HETs (WT vs. KO: P<0.00016; HET vs. KO: P<0.00001; Fig. 3N). Further analysis revealed a significant difference in sex in the rotarod test. Female KO mice displayed decreased latency to fall compared to WT mice (WT vs KO: P<0.003; Fig. 3O). Male HET mice showed a significant increase in time spent on the rotarod compared to WT mice, particularly on the second day of testing (WT vs. HET: P<1.79e–7; Fig. 3P).

We next assessed auditory startle responses and sensorimotor gating. All three groups displayed the same levels of acoustic startle response to a range of auditory stimuli from 0 to 120 dB (Fig. 3Q) and completely normal PPI (Fig. 3R).

Shank3E13 KO Mice Display Deficits in Spatial Learning

A significant percentage of patients with autism have comorbid intellectual disability [Leyfer et al., 2006; Srivastava & Schwartz, 2014], the prevalence of which is even higher in PMS [Phelan & Rogers, 1993]. Thus, we tested spatial learning and memory ability in Shank3^{E13} mutants using the Morris water maze. Shank3^{E13} KO mice displayed a significantly increased latency to reach the hidden platform compared to WT and HET (WT vs. KO: P<6.52E-09; HET vs. KO: P<0.0004; Fig. 4A). Using distance traveled prior to reaching the target platform, a measure that eliminates swim speed as a confound, KO mice also traveled longer distances during training compared to WT and HET mice (WT vs. KO: P<1.1E-16, HET vs. KO: P<1.8E-9; Fig. 4B). Consistent with decreased transition to a spatial learning strategy, KO mice spent more time in the periphery or thigmotaxis zone (WT vs. KO: P<2.1E-8, HET vs. KO: P<0.003; Fig. 4C). During the probe test for spatial memory 24 hr following the final training session, Shank3^{E13} KOs displayed no significant preference for the target quadrant, while both WT and HET mice showed clear spatial preferences (WT vs. KO: P<0.005; Fig. 4D).

Intact Basal Synaptic Transmission and Short-Term Plasticity at Hippocampal Synapses in Shank3E13 HET and KO Mice

Because spatial learning is known to be dependent on hippocampal function and plasticity [Morris, Garrud, Rawlins, & O'Keefe, 1982; Moser & Moser, 1998; Moser, Krobert, Moser, & Morris, 1998] we examined these in Shank3^{E13} mutants. We first measured basal synaptic transmission using input/output (I/O) curves to measure responsiveness of CA1 pyramidal neurons to Schaffer collateral stimulation at 0.05 Hz (Fig. 5A). We found no difference between WT and Shank3^{E13} HET or KO mice for field excitatory postsynaptic potential (fEPSP) slope vs. stimulus intensity (Two-Way RM ANOVA. Genotype: P=0.2407; Stimulus Intensity: P<0.0001; Genotype×Stimulus Intensity: P=0.8857) or fEPSP slope vs. fiber

volley amplitude (Two-Way RM ANOVA. Genotype: P=0.6258; Stimulus Intensity: P<0.0001; Genotype×Stimulus Intensity: P=0.9673).

We also examined short-term plasticity as an indicator of presynaptic function. Paired-pulse ratio (PPR) was measured at 0.05Hz with interstimulus intervals (ISI) 30–500 msec in pseudorandom order (Fig. 5B). Stimulus intensity was set at 50% of the maximum fEPSP and adjusted to prevent epileptiform activity at shorter interstimulus intervals. The average of five trials at each ISI is reported per slice. However, no difference in PPR was found at any ISI (Two-Way RM ANOVA. Genotype: P = 0.4139; ISI: P<0.0001; Genotype X ISI: P=0.3638).

Shank3E13 HET and KO Mice Exhibit Impaired Hippocampal Long-Term Potentiation

Next we investigated NMDA receptor-dependent long-term potentiation (LTP) and Group I mGluR-dependent long-term depression (mGluR-LTD). Stimulus intensity was adjusted to generate 50–75% of the maximum fEPSP for LTP, and a stable baseline was recorded for 20 min prior to the 1-sec, 100 Hz conditioning stimulus (Fig. 5C). Potentiation was measured as the average fEPSP slope at 55–60 min post-tetanus normalized to the average fEPSP of the baseline (Fig. 5D). We observed significantly decreased LTP in Shank3^{E13} HET and KO mice (One-Way ANOVA, P=0.0438), indicating that NMDA receptor-mediated LTP is impaired in these mice and may underlie hippocampus-dependent learning and memory deficits.

Increases [Huber, Gallagher, Warren, & Bear, 2002] and decreases [Bateup, Takasaki, Saulnier, Denefrio, & Sabatini, 2011] in LTD induced by application of Group 1 mGluR agonists have been identified in genetic models of autism. Furthermore, Group I mGluRs, as well as AMPARs and NMDARs, are being targeted for their therapeutic potential in ASD [Connor, Bariselli, & Bellone, 2014]. To determine whether Group I mGluR function is altered in Shank3^{E13} mutants 100μM DHPG was bath applied for 10min and LTD was determined as the average fEPSP at 55–60 min following the start of DHPG washout, normalized to the average baseline fEPSP (Fig. 5E). LTD was similar across all three genotypes (Fig. 5F), indicating no effect on Group I mGluR-mediated long-term plasticity (One-Way ANOVA, P=0.5382).

NMDAR/AMPAR Ratio is Decreased in Dorsal Striatum of Shank3E13 Mice

Shank3^{E13} HET and KO mice demonstrate increased repetitive grooming behavior, an obsessive-compulsive disorder-like phenotype attributed, in part, to deficits in striatal synaptic transmission in SAPAP3 mutant mice [Wan, Feng, & Calakos, 2011; Wan et al., 2014; Welch et al., 2007]. To determine whether abnormal striatal synaptic transmission correlates with repetitive grooming in Shank3^{E13} HET and KO mice, we used intrastriatal stimulation to evoke EPSCs from MSNs of dorsal striatum. Stimulus intensity (230–250 μA) was set to generate 200–500 pA peak amplitude of AMPAR-mediated currents at −70 mV holding potential. After achieving a stable baseline (5–10 min), 20 consecutive traces were recorded at 0.1 Hz, and peak amplitude measured 10–15 msec after stimulus onset was taken as the AMPAR-mediated component of the EPSC. Holding potential was gradually increased to +40 mV and the NMDAR-mediated component of the EPSC was measured at

40 msec following stimulus onset. The resulting NMDA/AMPA ratio was lower in MSNs from Shank3^{E13} HET and KO mice compared to WT [One-Way ANOVA, $P<0.0001$; Bonferroni's multiple comparisons. $P<0.001$ (WT vs. HET), $P<0.05$ (WT vs. KO)] as shown in mean NMDA/AMPA ratio (Fig. 6A) and in representative traces (Fig. 6B). Thus baseline synaptic function is altered in striatum due to either decreased NMDAR-mediated responses or increased AMPAR-mediated responses.

Altered Protein Expression in Striatal Tissue Lysates from Shank3E13 Mutants

To further delineate the impaired baseline striatal synaptic function in the Shank3^{E13} mutant mice, we investigated striatal protein expression levels focusing on synaptic proteins that interact directly or indirectly with Shank3. Whole tissue lysates from striatal tissue showed a significant reduction in GluN1 (WT vs. KO $P<0.01$), Homer 1b/c (WT vs. KO $P<0.006$) and PSD-95 (WT vs. KO $P<0.001$) in Shank3^{E13} KO mice compared to WT mice (Fig. 7A). Shank3^{E13} HET mice also show a trend toward a decrease in GluN1 (WT vs. HET $P=0.078$; Fig. 7A). To determine whether synaptosomal protein expression was altered in Shank3^{E13} mutant mice, we used striatal synaptosome preparations and observed a significant reduction in GluA2 (WT vs. KO $P<0.006$), GluA3 (WT vs. KO $P<0.016$), GluN2A (WT vs. KO $P<0.005$), GluN2B (WT vs. KO $P<0.046$), Homer 1 b/c (WT vs. KO $P<0.0001$), and PSD-95 (WT vs. KO $P<0.0033$) in Shank3^{E13} KO mice compared to WT mice (Fig. 7B). Shank3^{E13} HET mice also show a decrease in GluN2B (WT vs. HET $P<0.038$), Homer 1 b/c (WT vs. HET $P<0.0351$), and PSD-95 (WT vs. HET $P<0.0288$) when compared to WT. To determine whether synaptosomal protein expression was also altered in Shank3^{E13} mutant mice, we used hippocampal synaptosome preparations and observed a significant reduction in GluA1 (WT vs. HET $P<0.03$) and GluN1 (WT vs. HET $P<0.03$) in Shank3^{E13} HET mice compared to WT mice (Fig. 7C). Thus, our biochemical studies indicate that synaptic protein composition is altered in the striatum of both Shank3^{E13} HET and KO and the hippocampus of Shank3^{E13} HET mice.

Discussion

We target deletion of *Shank3's* PDZ domain by inserting a premature stop codon in *Shank3* prior to exon 13. An additional feature of this model is that the neo-Stop cassette is flanked by loxP sites, allowing future studies to feature regional and temporal control over the mutation. We show that this genetic disruption results in loss of the two highest molecular weight isoforms of Shank3 along with behaviors with face validity for ASD, deficits in hippocampal plasticity, altered striatal glutamatergic synaptic transmission, and altered synaptic glutamate receptor subunit expression.

We should note that while generating our Shank3^{E13} mutant mouse, another group successfully generated and published a similar mouse and characterized the homozygous knockout [Peca et al., 2011]. Thus, our study confirms and expands on the deficits described in the homozygous state [Peca et al., 2011]. The present study, however, represents the first characterization of the more clinically relevant heterozygous mutant model in which multiple important phenotypes were discovered.

Both Shank3^{E13} HET and KO mice displayed increase repetitive grooming and social deficits. Peca et al. found increased grooming behaviors to varying degrees in 35% of their homozygous mice colony that led to skin lesions [Peca et al., 2011]. [Schmeisser et al., 2012] also observed skin lesions in a similar Shank3 mutant mouse model in which the PDZ domain was disrupted. Curiously, we found that marble burying was not increased, but rather decreased in both heterozygous and homozygous mutants. Such decreased marble burying has been observed by us in other Shank3 mutant models [Kouser et al., 2013; Speed et al., 2015]. We observed increased grooming but no consistent skin lesions in our mutants. We also did not observe an anxiety-like phenotype in our mutant mice. Further validating the lack of anxiety in our mutant mice was the decrease in rearing observed in both HET and KO mice. Decreased rearing was also observed in the homozygous mice in Peca et al. [2011]. Additionally, we observed differences in motor learning and spatial memory in Shank3^{E13} KO mice that differ from similar studies in Peca et al. [2011]. Our deficits in Shank3^{E13} KO motor learning were observed on the second day of rotarod testing, whereas [Peca et al., 2011] did not conduct a second day of testing. It may be of interest that initial coordination on day one of the rotarod was decreased in both heterozygotes and homozygotes, while heterozygotes seems to have improved motor learning retention on day 2 of testing. Additionally Peca et al. did not use females in their behavioral testing [Peca et al., 2011], and the females appeared to drive rotarod differences in our model. Differences in protocol and cohort makeup were also present in the Morris water maze in which we observe spatial memory deficits in Shank3^{E13} KOs not seen in Peca et al. [2011]. Differences in the two studies may have also manifested as a result of the two different breeding and housing strategies. Our Shank3^{E13} mice were generated from 12 heterozygous breeding pairs generating littermate triplets (WT/HET/KO) or littermate pairs (WT/HET; WT/KO). Peca et al. generated their behavioral cohort from homozygous breeder pairs (WT×WT, KO×KO) [Peca et al., 2011]. Also, [Peca et al., 2011] housed mice by genotype, whereas we housed mice as littermate triplets or pairs to ensure that environmental variables are equally experienced. Subtle genetic background differences or differences in stress levels and husbandry conditions could also contribute to observed differences.

Regardless of the differences, we both demonstrated altered behaviors with ASD face validity in our models. Thus, where homozygous mutants are concerned, our two studies largely replicate across similar tests and should be viewed as complimentary.

Perhaps more important is our characterization of the clinically relevant heterozygous Shank3^{E13} mutants. Shank3^{E13} HET mice demonstrate a robust increase in repetitive grooming and deficits in social tasks including social preference and social recognition of a juvenile mouse. A lack of social preference in the HET but not the KO further supports the importance of characterizing the heterozygous mouse model and suggests variation in gene expression can contribute to heterogeneity in phenotypes.

In addition, we observed lack of sociability in the heterozygotes, but not the homozygotes. This is a puzzling observation but may be explained by differential compensation in the heterozygotes vs. homozygotes by other Shank isoforms. Direct interaction between two freely moving mice provides a more reciprocal interaction and was abnormal in homozygous Shank3^{E13} mutants. While this and other mutant mouse studies involving *Shank3*

truncations seem to mimic some of the behavioral phenotypes observed in ASD and PMS (incoordination, learning and memory deficits, repetitive behaviors, and social deficits), the phenotypes among mouse models and even patients with Shank3 can be highly variable. More clinical data are needed on genotype/phenotype relationships in patients with complete deletion of Shank3 vs. mutations in order to further determine how different Shank3 mutations affect behavior in patients [Harony-Nicolas, De Rubeis, Kolevzon, & Buxbaum, 2015].

In eight of our behavioral tests, we identified a main effect of sex that is consistent with overall differences in behavior between males and females in some paradigms. Only in rearing, locomotor activity, and rotarod was there an actual interaction between genotype and sex. This is consistent with roughly equal male/female ratios in patients with Phelan-McDermid Syndrome.

Our study also demonstrates deficits in CA1 hippocampal LTP in Shank3^{E13} HET and KO mice. Deficits in LTP have been fairly consistently observed across multiple Shank3 mouse models [Bozdagi et al., 2010; Jaramillo et al., 2015; Kouser et al., 2013; Yang et al., 2012].

Additionally, Shank3^{E13} HET and KO mice demonstrate deficits in striatal NMDAR/AMPAR-ratio in dorsal striatum. We also observed reduction in glutamatergic receptors including GluA2, GluA3, GluN2A, and GluN2B in western blots from Shank3^{E13} KO mice synaptosomes, a finding similar to that presented in Peca et al. [2011]. Furthermore, Shank3^{E13} HET mice displayed a reduction in synaptosomal GluN2B.

Overall, this study identifies the first robust, ASD-relevant behavioral abnormalities in the heterozygous model of a Shank3 PDZ domain mutant. We find clear differences in striatal synaptic function in heterozygous mice for the first time. In terms of the homozygous mutants, we feel this study compliments and extends Peca et al. [2011] and other publications involving mutation/deletion of *Shank3*. Thus, our study provides behavioral, biochemical, and physiological alterations in a clinically relevant *Shank3* mutant model. Furthermore, this model was created with the ability to genetically reverse the mutation, providing a means to examine both regional and temporal genetic rescue of the identified phenotypes in future studies. We note that a key finding in a similar Shank3 mutant model has recently been published demonstrating that some behavioral and other phenotypes can be reversed by adult-onset temporal reversal of Shank3 deletion/mutation [Mei et al., 2016]. Replication of such groundbreaking findings across laboratories and in multiple Shank3 mutant mouse models will be key to move the field forward toward novel therapeutics.

Acknowledgments

We thank Dr. Paul Worley for Shank3 antibody. Also to Dr. Yong-hui Jiang for providing whole brains from complete Shank3 knockouts. Supported by NIH (R01HD069560, R21HD065290, & R01HD069560-S1 to C.M.P.), Autism Speaks (C.M.P.), Autism Speaks and Autism Science Foundation Postdoctoral Fellowships (HES), The Hartwell Foundation (C.M.P.), Ed and Sue Rose Distinguished Professorship in Neurology (C.M.P.), and gifts from Drs. Clay Heighten and Debra Caudy and BRAINS for Autism (C.M.P.). C.M.P. has accepted travel funds and honoraria to speak once at each of the following companies: Psychogenics, Inc.; Astra-Zeneca; Roche; Pfizer; and Dainippon Sumitomo Pharma Co. Dr. Powell also has investigator-initiated grant funding through a contract for clinical research with Novartis.

References

Arons MH, Thynne CJ, Grabrucker AM, Li D, Schoen M, Cheyne JE, et al. Autism-associated mutations in ProSAP2/Shank3 impair synaptic transmission and neurexin-neuroligin-mediated transsynaptic signaling. The Journal of Neuroscience : The Official Journal of the Society for Neuroscience. 2012; 32:14966–14978. [PubMed: 23100419]

Bateup HS, Takasaki KT, Saulnier JL, Denefrio CL, Sabatini BL. Loss of Tsc1 in vivo impairs hippocampal mGluR-LTD and increases excitatory synaptic function. Journal of Neuroscience. 2011; 31:8862–8869. [PubMed: 21677170]

Blundell J, Blaiss CA, Etherton MR, Espinosa F, Tabuchi K, Walz C, et al. Neuroligin-1 deletion results in impaired spatial memory and increased repetitive behavior. The Journal of Neuroscience : The Official Journal of the Society for Neuroscience. 2010a; 30:2115–2129. [PubMed: 20147539]

Blundell J, Kaeser PS, Sudhof TC, Powell CM. RIM1alpha and interacting proteins involved in presynaptic plasticity mediate prepulse inhibition and additional behaviors linked to schizophrenia. The Journal of Neuroscience : The Official Journal of the Society for Neuroscience. 2010b; 30:5326–5333. [PubMed: 20392954]

Blundell J, Tabuchi K, Bolliger MF, Blaiss CA, Brose N, Liu X, et al. Increased anxiety-like behavior in mice lacking the inhibitory synapse cell adhesion molecule neuroligin 2. Genes, Brain, and Behavior. 2009; 8:114–126.

Boeckers TM, Bockmann J, Kreutz MR, Gundelfinger ED. ProSAP/Shank proteins: A family of higher order organizing molecules of the postsynaptic density with an emerging role in human neurological disease. Journal of Neurochemistry. 2002; 81:903–910. [PubMed: 12065602]

Bonaglia MC, Giorda R, Borgatti R, Felisari G, Gagliardi C, Selicorni A, Zuffardi O. Disruption of the ProSAP2 gene in a t(12;22)(q24.1;q13.3) is associated with the 22q13.3 deletion syndrome. The American Journal of Human Genetics. 2001; 69:261–268. [PubMed: 11431708]

Bozdagi O, Sakurai T, Papapetrou D, Wang X, Dickstein DL, Takahashi N, et al. Haploinsufficiency of the autism-associated Shank3 gene leads to deficits in synaptic function, social interaction, and social communication. Molecular Autism. 2010; 1:15. [PubMed: 21167025]

Dragatsis I, Zeitlin S. A method for the generation of conditional gene repair mutations in mice. Nucleic Acids Research. 2001; 29:E10. [PubMed: 11160912]

Duffney LJ, Wei J, Cheng J, Liu W, Smith KR, Kittler JT, Yan Z. Shank3 deficiency induces NMDA receptor hypofunction via an actin-dependent mechanism. The Journal of Neuroscience: The Official Journal of the Society for Neuroscience. 2013; 33:15767–15778. [PubMed: 24089484]

Durand CM, Betancur C, Boeckers TM, Bockmann J, Chaste P, Fauchereau F, et al. Mutations in the gene encoding the synaptic scaffolding protein SHANK3 are associated with autism spectrum disorders. Nature Genetics. 2007; 39:25–27. [PubMed: 17173049]

Ehlers MD. Synapse structure: Glutamate receptors connected by the shanks. Current Biology. 1999; 9:R848–R850. [PubMed: 10574750]

Ehlers MD. Molecular morphogens for dendritic spines. Trends Neuroscience. 2002; 25:64–67.

Etherton MR, Blaiss CA, Powell CM, Sudhof TC. Mouse neurexin-1alpha deletion causes correlated electrophysiological and behavioral changes consistent with cognitive impairments. Proceedings of the National Academy of Sciences of the United States of America. 2009; 106:17998–18003. [PubMed: 19822762]

Gauthier J, et al. De novo mutations in the gene encoding the synaptic scaffolding protein SHANK3 in patients ascertained for schizophrenia. Proceedings of the National Academy of Sciences of the United States of America. 2010; 107:7863–7868. [PubMed: 20385823]

Gong Y, Lippa CF, Zhu J, Lin Q, Rosso AL. Disruption of glutamate receptors at Shank-postsynaptic platform in Alzheimer's disease. Brain Research. 2009; 1292:191–198. [PubMed: 19635471]

Grabrucker S, Proepper C, Mangus K, Eckert M, Chhabra R, Schmeisser MJ, et al. The PSD protein Pro-SAP2/Shank3 displays synapto-nuclear shuttling which is deregulated in a schizophrenia-associated mutation. Experimental Neurology. 2014; 253:126–137. [PubMed: 24382453]

Guilmatre A, Huguet G, Delorme R, Bourgeron T. The emerging role of SHANK genes in neuropsychiatric disorders. Developmental Neurobiology. 2014; 74:113–122. [PubMed: 24124131]

Guy J, Gan J, Selfridge J, Cobb S, Bird A. Reversal of neurological defects in a mouse model of Rett syndrome. Science. 2007; 315:1143–1147. [PubMed: 17289941]

Han K, Holder JL Jr, Schaaf CP, Lu H, Chen H, Kang H, et al. SHANK3 overexpression causes manic-like behaviour with unique pharmacogenetic properties. Nature. 2013; 503:72–77. [PubMed: 24153177]

Harony-Nicolas H, De Rubeis S, Kolevzon A, Buxbaum JD. Phelan McDermid syndrome: From genetic discoveries to animal models and treatment. Journal of Child Neurology. 2015; 30:1861–1870. [PubMed: 26350728]

Herbert MR. SHANK3, the synapse, and autism. The New England Journal of Medicine. 2011; 365:173–175. [PubMed: 21751912]

Huber KM, Gallagher SM, Warren ST, Bear MF. Altered synaptic plasticity in a mouse model of fragile X mental retardation. Proceeding of National Academic Science United States of Amaerica. 2002; 99:7746–7750.

Jaramillo TC, Speed HE, Xuan Z, Reimers JM, Lui S, Powell C. Altered striatal synaptic function and abnormal behaviour in Shank3 exon4–9 deletion mouse model of autism. Autism Research. 2015 in press.

Jaramillo TC, Speed HE, Xuan Z, Reimers JM, Liu S, Powell CM. Altered striatal synaptic function and abnormal behaviour in Shank3 exon4–9 deletion mouse model of autism. Autism Research. 2016; 9:350–375. [PubMed: 26559786]

Kolevzon A, Cai G, Soorya L, Takahashi N, Grodberg D, Kajiwara Y, et al. Analysis of a purported SHANK3 mutation in a boy with autism: Clinical impact of rare variant research in neurodevelopmental disabilities. Brain Research. 2011; 1380:98–105. [PubMed: 21062623]

Kouser M, Speed HE, Dewey CM, Reimers JM, Widman AJ, Gupta N, et al. Loss of predominant shank3 isoforms results in hippocampus-dependent impairments in behavior and synaptic transmission. The Journal of Neuroscience : The Official Journal of the Society for Neuroscience. 2013; 33:18448–18468. [PubMed: 24259569]

Kwon CH, Luikart BW, Powell CM, Zhou J, Matheny SA, Zhang W, et al. Pten regulates neuronal arborization and social interaction in mice. Neuron. 2006; 50:377–388. [PubMed: 16675393]

Leyfer OT, Folstein SE, Bacalman S, Davis NO, Dinh E, Morgan J, et al. Comorbid psychiatric disorders in children with autism: Interview development and rates of disorders. Journal of Autism and Developmental Disorders. 2006; 36:849–861. [PubMed: 16845581]

Mei Y, Monteiro P, Zhou Y, Kim JA, Gao X, Fu Z, Feng G. Adult restoration of Shank3 expression rescues selective autistic-like phenotypes. Nature. 2016; 530:481–484. [PubMed: 26886798]

Misceo D, Rodningen OK, Baroy T, Sorte H, Mellembakken JR, Stromme P, et al. A translocation between Xq21.33 and 22q13.33 causes an intragenic SHANK3 deletion in a woman with Phelan-McDermid syndrome and hypergonadotropic hypogonadism. American Journal of Medical Genetics A. 2011; 155A:403–408.

Moessner R, Marshall CR, Sutcliffe JS, Skaug J, Pinto D, Vincent J, et al. Contribution of SHANK3 mutations to autism spectrum disorder. American Journal of Human Genetics. 2007; 81:1289–1297. [PubMed: 17999366]

Morris RG, Garrud P, Rawlins JN, Keefe J. Place navigation impaired in rats with hippocampal lesions. Nature. 1982; 297:681–683. [PubMed: 7088155]

Moser EI, Krobert KA, Moser MB, Morris RG. Impaired spatial learning after saturation of long-term potentiation. Science. 1998; 281:2038–2042. [PubMed: 9748165]

Moser MB, Moser EI. Functional differentiation in the hippocampus. Hippocampus. 1998; 8:608–619. [PubMed: 9882018]

Moy SS, Nadler JJ, Perez A, Barbaro RP, Johns JM, Magnuson TR, et al. Sociability and preference for social novelty in five inbred strains: An approach to assess autistic-like behavior in mice. Genes Brain and Behavior. 2004; 3:287–302.

Nadler JJ, Moy SS, Dold G, Trang D, Simmons N, Perez A, et al. Automated apparatus for quantitation of social approach behaviors in mice. Genes Brain and Behavior. 2004; 3:303–314.

Naisbitt S, Kim E, Tu JC, Xiao B, Sala C, Valtschanoff J, et al. Shank, a novel family of postsynaptic density proteins that binds to the NMDA receptor/PSD-95/GKAP complex and cortactin. Neuron. 1999; 23:569–582. [PubMed: 10433268]

Connor EC, Bariselli S, Bellone C. Synaptic basis of social dysfunction: A focus on postsynaptic proteins linking group-I mGluRs with AMPARs and NMDARs. The European Journal of Neuroscience. 2014; 39:1114–1129. [PubMed: 24712991]

Park E, Na M, Choi J, Kim S, Lee JR, Yoon J, et al. The Shank family of postsynaptic density proteins interacts with and promotes synaptic accumulation of the beta PIX guanine nucleotide exchange factor for Rac1 and Cdc42. Journal of Biological Chemistry. 2003; 278:19220–19229. [PubMed: 12626503]

Peca J, Feliciano C, Ting JT, Wang W, Wells MF, Venkatraman TN, et al. Shank3 mutant mice display autistic-like behaviours and striatal dysfunction. Nature. 2011; 472:437–442. [PubMed: 21423165]

Phelan, K., Rogers, RC. Phelan-McDermid syndrome. Pagon, RA.Adam, MP.Ardinger, HH.Bird, TD.Dolan, CR.Fong, CT.Smith, RJH., Stephens, K., editors. Seattle (WA): GeneReviews(R); 1993.

Powell CM, Schoch S, Monteggia L, Barrot M, Matos MF, Feldmann N, et al. The presynaptic active zone protein RIM1alpha is critical for normal learning and memory. Neuron. 2004; 42:143–153. [PubMed: 15066271]

Roussignol G, Ango F, Romorini S, Tu JC, Sala C, Worley PF, et al. Shank expression is sufficient to induce functional dendritic spine synapses in aspiny neurons. Journal of Neuroscience. 2005; 25:3560–3570. [PubMed: 15814786]

Sarasua SM, Dwivedi A, Boccuto L, Rollins JD, Chen CF, Rogers RC, et al. Association between deletion size and important phenotypes expands the genomic region of interest in Phelan-McDermid syndrome (22q13 deletion syndrome). Journal of Medical Genetics. 2011; 48:761–766. [PubMed: 21984749]

Schmeisser MJ, Ey E, Wegener S, Bockmann J, Stempel AV, Kuebler A, et al. Autistic-like behaviours and hyperactivity in mice lacking ProSAP1/Shank2. Nature. 2012; 486:256–260. [PubMed: 22699619]

Shetreat-Klein M, Shinnar S, Rapin I. Abnormalities of joint mobility and gait in children with autism spectrum disorders. Brain & #Development. 2014; 36:91–96. [PubMed: 22401670]

Soorya L, Kolevzon A, Zweifach J, Lim T, Dobry Y, Schwartz L, et al. Prospective investigation of autism and genotype-phenotype correlations in 22q13 deletion syndrome and SHANK3 deficiency. Molecular Autism. 2013; 4:18. [PubMed: 23758760]

Speed HE, Kouser M, Xuan Z, Reimers JM, Ochoa CF, Gupta N, et al. Autism-associated insertion mutation (InsG) of Shank3 exon 21 causes impaired synaptic transmission and behavioral deficits. Journal of Neuroscience. 2015; 35:9648–9665. [PubMed: 26134648]

Srivastava AK, Schwartz CE. Intellectual disability and autism spectrum disorders: causal genes and molecular mechanisms. Neuroscience and Biobehavioral Reviews. 2014; 46(Pt 2):161–174. [PubMed: 24709068]

Tabuchi K, Blundell J, Etherton MR, Hammer RE, Liu X, Powell CM, Sudhof TC. A neuroligin-3 mutation implicated in autism increases inhibitory synaptic transmission in mice. Science. 2007; 318:71–76. [PubMed: 17823315]

Tu JC, Xiao B, Naisbitt S, Yuan JP, Petralia RS, Brakeman P, et al. Coupling of mGluR/Homer and PSD-95 complexes by the Shank family of postsynaptic density proteins. Neuron. 1999; 23:583–592. [PubMed: 10433269]

Verpelli C, Dvoretskova E, Vicidomini C, Rossi F, Chiappalone M, Schoen M, et al. Importance of Shank3 protein in regulating metabotropic glutamate receptor 5 (mGluR5) expression and signaling at synapses. Journal of Biological Chemistry. 2011; 286:34839–34850. [PubMed: 21795692]

Vucurovic K, Landais E, Delahaigue C, Eutrope J, Schneider A, Leroy C, et al. Bipolar affective disorder and early dementia onset in a male patient with SHANK3 deletion. European Journal of Medical Genetics. 2012; 55:625–629. [PubMed: 22922660]

Wan Y, Ade KK, Caffall Z, Ilcim Ozlu M, Eroglu C, Feng G, Calakos N. Circuit-selective striatal synaptic dysfunction in the Sapap3 knockout mouse model of obsessive-compulsive disorder. Biological Psychiatry. 2014; 75:623–630. [PubMed: 23414593]

Wan Y, Feng G, Calakos N. Sapap3 deletion causes mGluR5-dependent silencing of AMPAR synapses. The Journal of Neuroscience : The Official Journal of the Society for Neuroscience. 2011; 31:16685–16691. [PubMed: 22090495]

Wang X, McCoy PA, Rodriguiz RM, Pan Y, Je HS, Roberts AC, et al. Synaptic dysfunction and abnormal behaviors in mice lacking major isoforms of Shank3. Human Molecular Genetics. 2011; 20:3093–3108. [PubMed: 21558424]

Wang X, Xu Q, Bey AL, Lee Y, Jiang YH. Transcriptional and functional complexity of Shank3 provides a molecular framework to understand the phenotypic heterogeneity of SHANK3 causing autism and Shank3 mutant mice. Molecular Autism. 2014; 5:30. [PubMed: 25071925]

Welch JM, Lu J, Rodriguiz RM, Trotta NC, Peca J, Ding JD, et al. Cortico-striatal synaptic defects and OCD-like behaviours in Sapap3-mutant mice. Nature. 2007; 448:894–900. [PubMed: 17713528]

Yang M, Bozdagi O, Scattoni ML, Wohr M, Roullet FI, Katz AM, et al. Reduced excitatory neurotransmission and mild autism-relevant phenotypes in adolescent Shank3 null mutant mice. The Journal of Neuroscience : the Official Journal of the Society for Neuroscience. 2012; 32:6525–6541. [PubMed: 22573675]

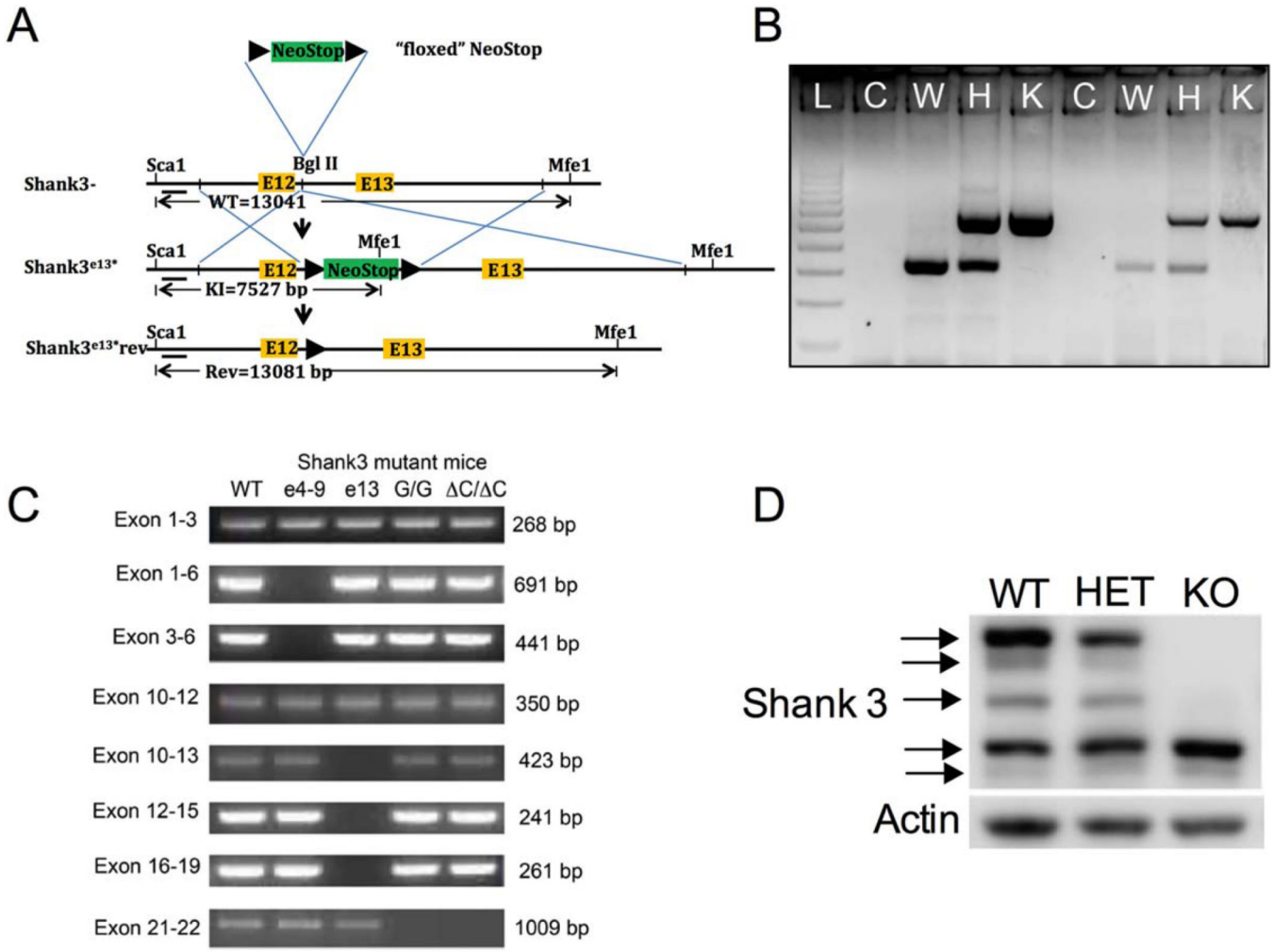

Figure 1.

Generation of Shank3^{E13} mice. (**A**) The schema showing the location of the Neo-Stop cassette within intron 12 (Bgl II) near WT exon 13 of *Shank3*, wild-type *Shank3* allele (Shank3-wt), product of homologous recombination (Shank3^{E13}*) and hypothetical genetic reversal (Shank3^{E13}*rev) by cre recombinase. The position of a Shank3 5′ flanking probe along with the size of diagnostic restriction fragments identifying the wild type, Shank3^{E13}* and Shank3^{E13}*rev are indicated. The restriction sites are: Sca1 and Mfe1. The black arrowheads represent loxP sites. (**B**) Genotyping analysis of WT (W), HET (H), and KO (K). WT mice produced a single 332 bp band while the KO produced a 576 bp band. HET produced bands of both sizes. A sample with no DNA was loaded as a control (C). "L" designates the 100bp ladder. (**C**) RT-PCR of cDNA from brain tissue of 4-week old (WT): wildtype, (e4–9):Shank3$^{e4–9}$ (Jaramillo et al., 2015a), (e13):Shank3^{e13}, (G/G):Shank3$^{G/G}$ (Speed et al., 2015), ΔC/ΔC: Shank3$^{ΔC/ΔC}$ (Kouser et al., 2013) mice. The *Shank3* gene contains five functional domains; Ankyrin binding domain from exons 4 to 9, SH3 domain from exons 11 to 12, PDZ domain from exons 14 to 16, Proline rich domain from exon 21, and SAM domain from exon 22. Shank3^{e13} mice show a loss of bands from exons 13 to 19 which indicates a lack of PDZ domain-encoding exons. Shank3$^{e4–9}$ shows a loss of bands

from exons 4 to 9. Shank3$^{G/G}$ and Shank3ΔC/ΔC show a loss of band containing exons 21–22. (**D**) Whole brain cell lysates from WT, HET, and KO Shank3^{E13} mice probed with C-terminal Shank3 antibody.

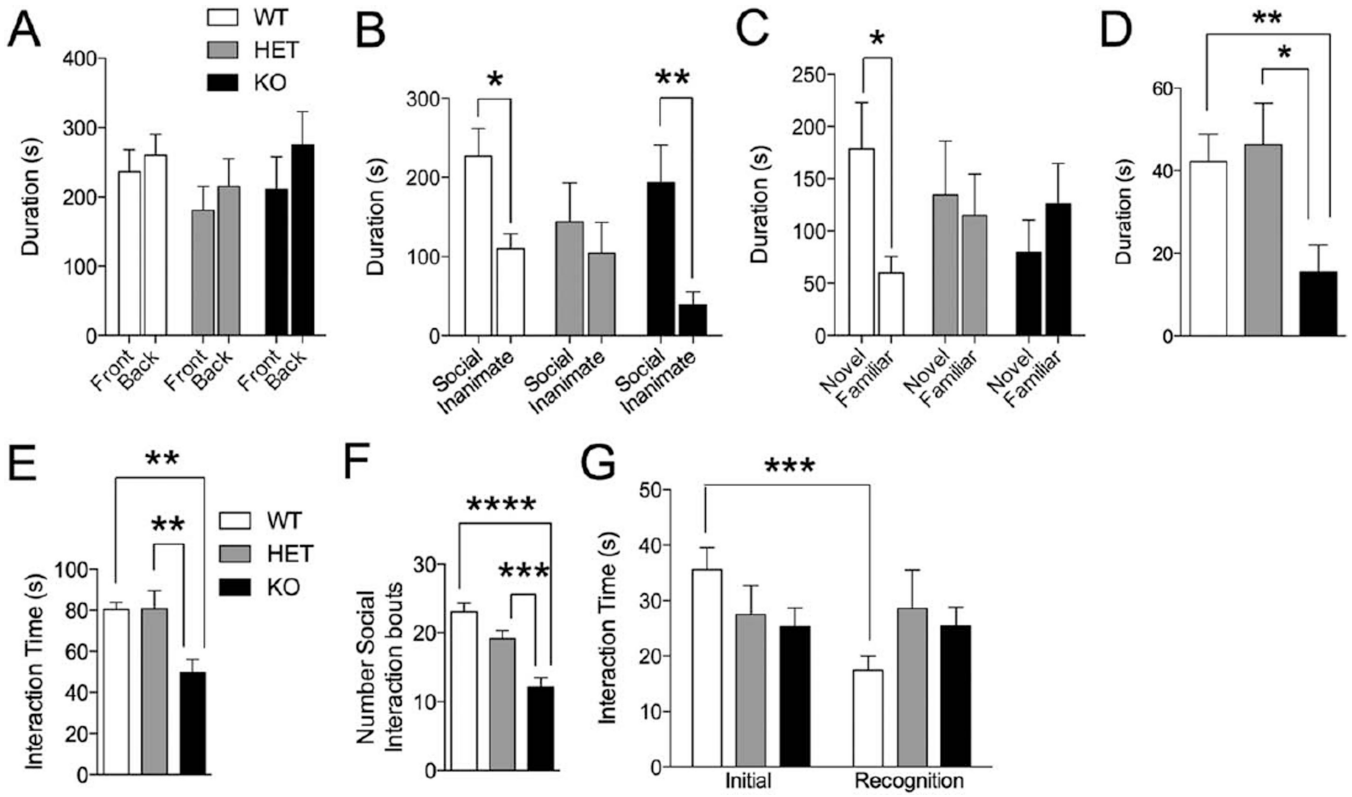

Figure 2.

Social test in Shank3^{E13} mutant mice. (**A**) In the 3-chamber test of sociability, none of the three mouse groups displayed an aberrant chamber preference in the initial trial. In second trial of this task, Shank3^{E13} HET mice did not display a preference for the social target over the inanimate object (**B**). In the third trial of this task, neither Shank3^{E13} HET nor KO mice displayed a preference for social novelty (**C**). Shank3^{E13} KO mice also displayed a significant decrease in approach of a novel, caged social target in the caged conspecific test (**D**). In the genotype and sex-matched social interaction test, Shank3^{E13} KO mice displayed a significant reduction in social interaction time (**E**), and a decrease in number of social bouts (**F**). Both HET and KO mice display deficits in social recognition in the social interaction with juvenile test of social memory (**G**). (*P<0.05; **P<0.01, ***P< 0.001, ****P< 0.0001; n = 20 WT, 20 HET, 15 KO).

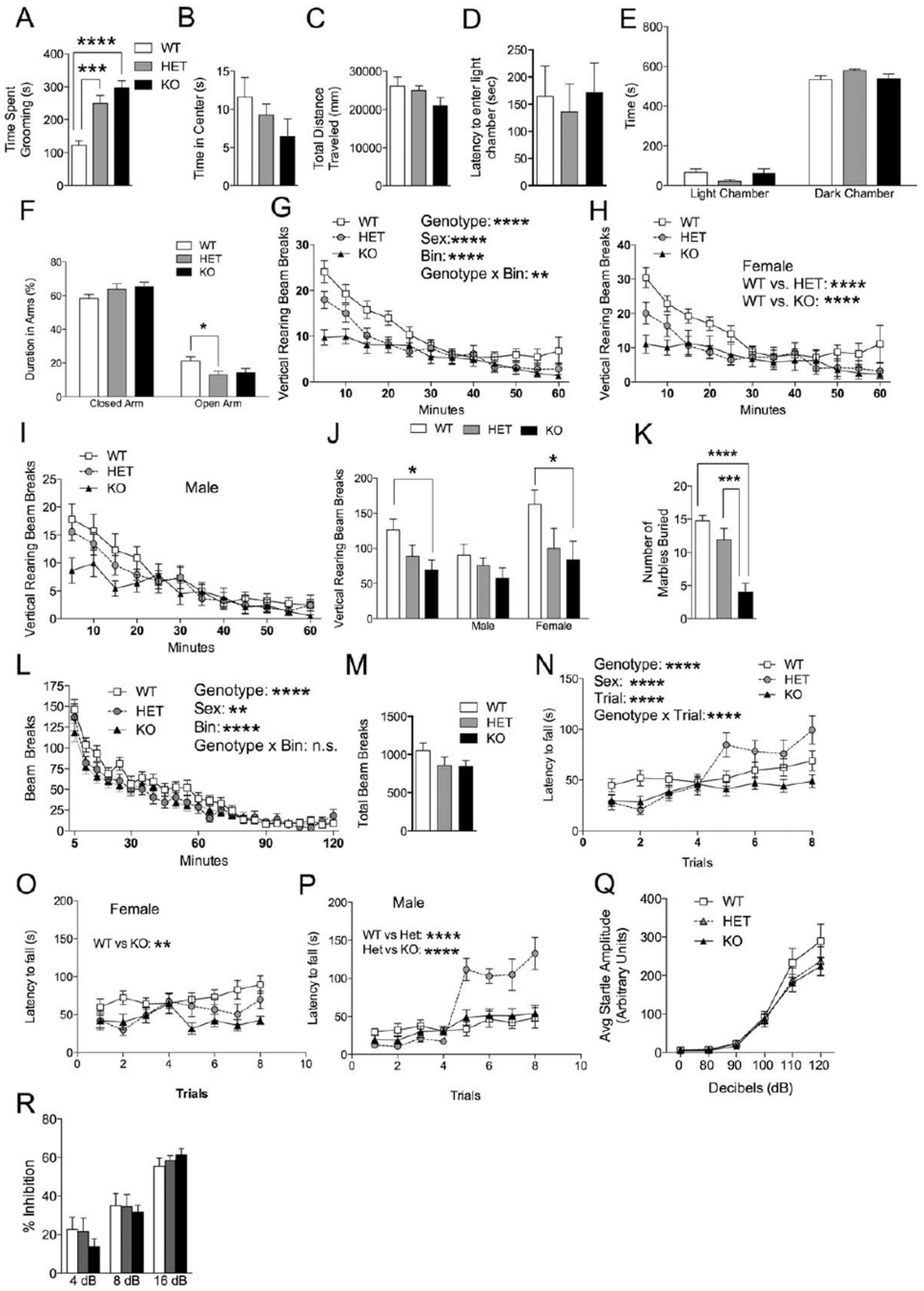

Figure 3.

Grooming, anxiety and motor behavior in Shank3^{E13} mutant mice. (**A**) Shank3^{E13} HET and KO mice displayed a significant increase in time spent grooming compared to WT littermate mice. In the open field test all genotypes spent similar time in the center (**B**). Additionally they all traveled similar distances (**C**). In the dark/light test all three genotypes had similar latencies to enter into the light chamber (**D**). All three genotypes spent a similar amount of time in light and dark chambers (**E**). In the elevated plus maze all three genotypes spent a similar percentage of time in the closed arms, however, there was a significant decrease in

time spent in the open arm in Shank3^{E13} HET mice when compared to WT mice (**F**). Shank3^{E13} HET and KO mice also displayed less rearing over a 1hr time period (**G**). Female Shank3^{E13} HET and KO mice displayed less rearing (**H**) while male mutant mice only displayed a trend toward less rearing (**I**). Total vertical rearing beam breaks was decreased in KO mice when analyzing the cohort. Further analysis revealed a decrease in female KO mice (**J**). In the marble-burying test Shank3^{E13} KO mice buried significantly less marbles than the WT and HET mice (**K**). In the locomotor test all three genotypes displayed similar levels of habituation over a 2-hr time period (**L**). There was no difference in the total number of beam breaks during the 2-hr locomotor test (**M**). In the rotarod test KO mice displayed decreased latency to fall compared to WT and HET mice (**N**). Female KO mice showed a significant decrease in latency to fall compared to WT (**O**). Male KO mice showed a significant decrease in latency to fall compared to HET and KO mice (**P**). All mouse groups displayed a similar startle response to auditory stimuli ranging from 0 to 120 db (**Q**). All three groups displayed similar % inhibition in the prepulse inhibition test (**R**). (*P<0.05, **P<0.01, ***P<0.001, n=20 WT, 20 HET, 15 KO).

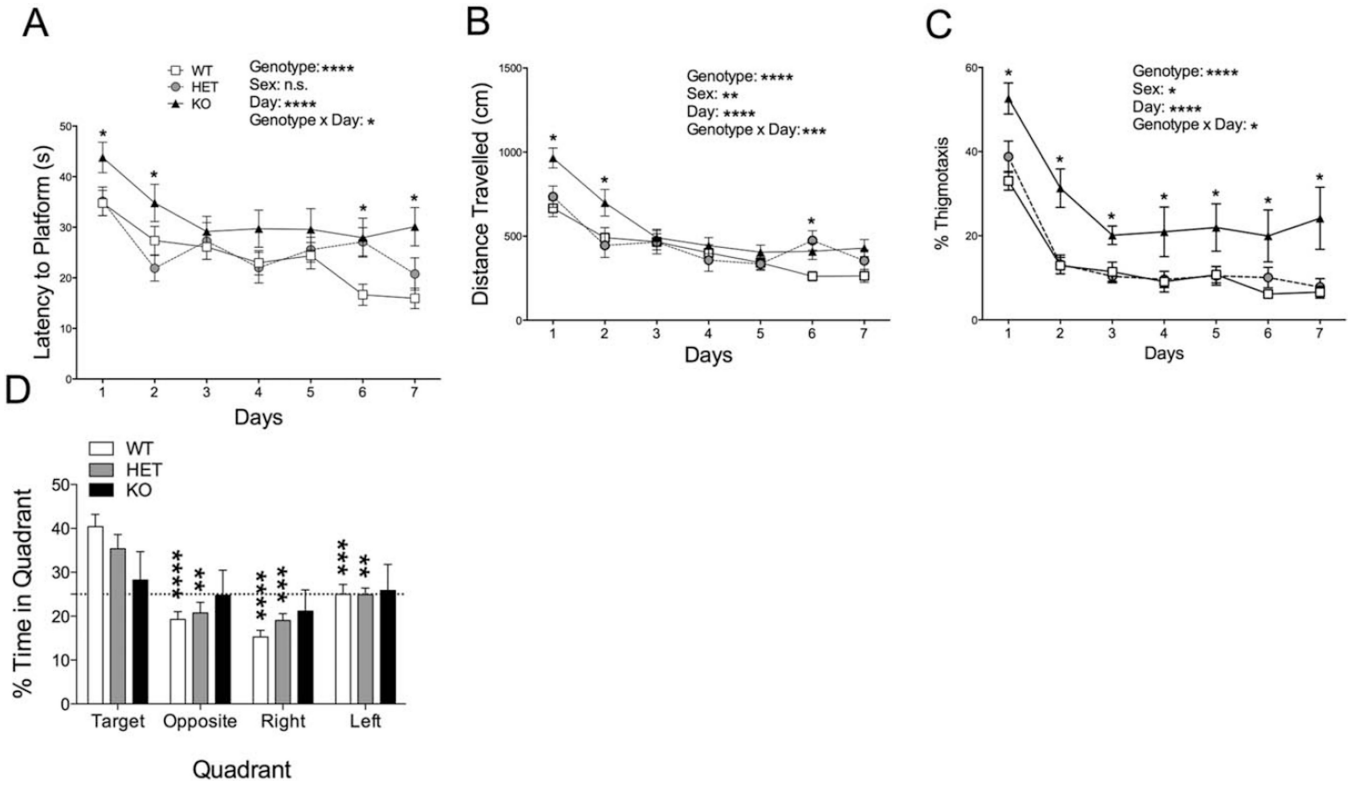

Figure 4.

Spatial learning behavior in Shank3^{E13} mutant mice. Shank3^{E13} KO mice displayed increased latency to reach the hidden platform (**A**, asterisks in graph near symbols refer to WT vs. KO). KO mice also displayed an increase in distance traveled before reaching the hidden platform (**B**, asterisks in graph near symbols refer to WT vs. KO) and % of time in thigmotaxis (**C**, asterisks in graph near symbols refer to WT vs. KO) during the training phase of the Morris water maze test. In the probe trial KO mice did not show a preference for the target quadrant compared to the other quadrants (**D**, asterisks in graph near bars denote comparison to Target quadrant within each group). (*P <0.05; **P<0.01, ***P <0.001, ****P<0.0001; n = 20 WT, 20 HET, 15 KO).

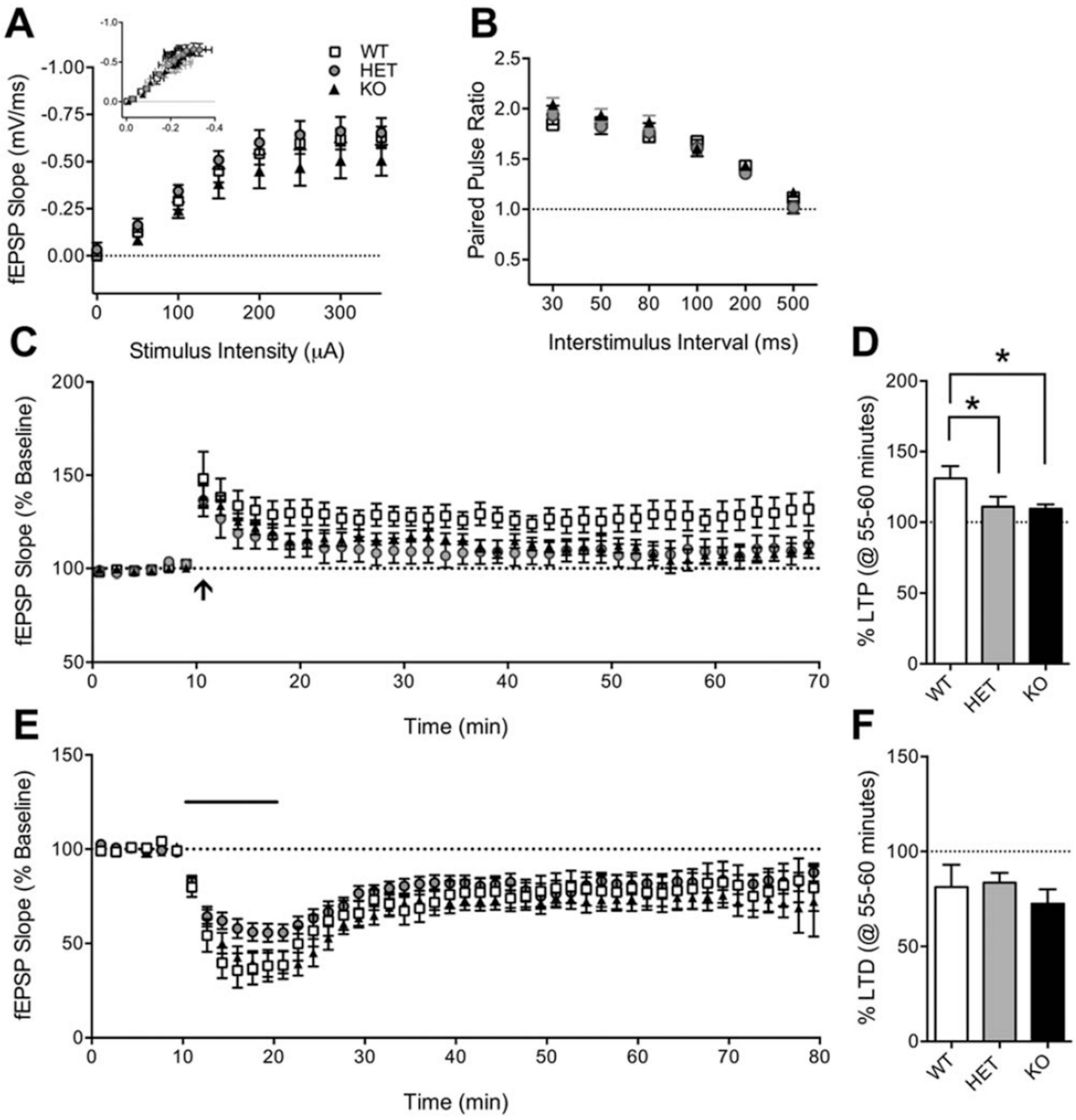

Figure 5.

Hippocampal synaptic function in Shank3^{E13} mice. (**A**) Input/output (I/O) curves show no effect of genotype on fEPSP slope at stimulus intensities 0–350 μA. Inset: fEPSP slope (mV/ms) plotted against fiber volley amplitude (mV). WT: 9 slices/6 mice, HET: 12 slices/7 mice, KO: 12 slices/7 mice. (**B**) Paired-pulse ratio (PPR, slope 2/slope 1) is not affected by the Shank3^{E13} mutation at interstimulus intervals 30–500 ms. WT: 8 slices/4 mice, HET: 14 slices/8 mice, KO: 17 slices/9 mice. (**C**) Long-term potentiation (LTP) induced by a single 1 sec, 100Hz train (arrow) is decreased in Shank3^{E13} HET and KO mice. Each data point is

shown as the average of five consecutive traces for clarity. (**D**) Mean normalized fEPSP at 55–60 min following conditioning stimulus showed decreased LTP in Shank3^{E13} HET and KO mice. WT: 11 slices/7 mice, Het: 9 slices/8 mice, KO: 12 slices/9 mice. (**E**) mGluR5-dependent long-term depression induced by 10-min bath application of Group I mGluR agonist DHPG (100 μM, solid bar) is not affected in Shank3^{E13} mutant mice. (**F**) Mean normalized fEPSP at 55–60 min following the start of DHPG washout showing normal mGluR-LTD in Shank3^{E13} mice. WT: 7 slices/5 mice, HET: 13 slices/8 mice, KO: 9 slices/6 mice. *P<0.05.

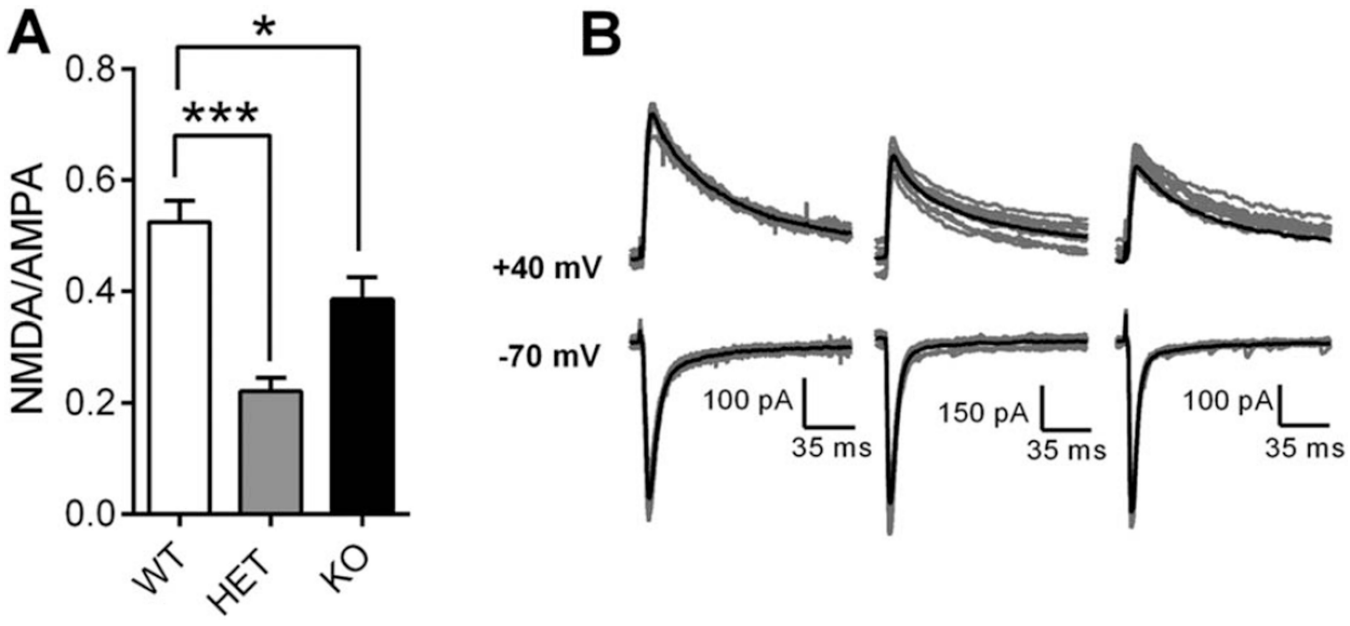

Figure 6.

Striatal synaptic transmission is altered in Shank3^{E13} mutant mice. (**A**) Mean NMDA/AMPA ratio is decreased in Shank3^{E13} HET and KO mice. (**B**) Ten consecutive raw traces (gray) with overlaid average traces (black) at −70 mV (bottom) and +40 mV (top) from WT (left), HET (middle), and KO (right) mice. WT: 28 cells/9 mice, HET: 18 cells/4 mice, KO: 25 cells/5 mice (*$P < 0.05$, **$P < 0.01$, ***$P < 0.001$).

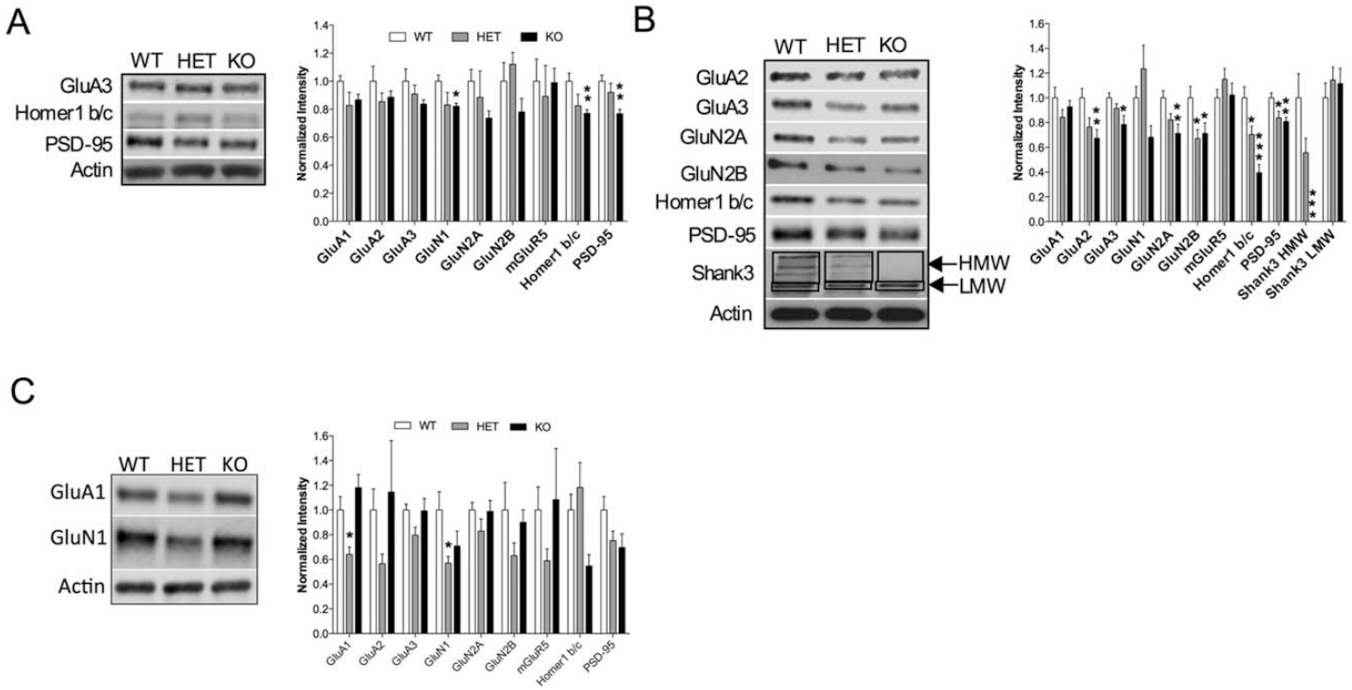

Figure 7.

Biochemical analysis of striatal and hippocampal synaptic proteins in Shank3^{E13} mutant mice. (**A**) Quantification of whole cell lysates derived from striatal tissue shows significant decreases in GluN1, Homer 1 b/c, and PSD-95. Sample blots are shown on the left with grouped data on the right. (**B**) Quantification of synaptosome preparations from striatal tissue shows significant decrease in GluA2, GluA3, GluN2A, GluN2B, Homer 1b/c, PSD-95, and Shank3 HMW bands (*P<0.05, **P<0.01, ***P<0.001; for whole cell lysates n=8 WT, 3 HET, 8 KO; for Synaptosome lysates n=16 WT, 11 HET, 16 KO for all samples except blots for Shank3 protein, n=8 WT, 8 HET, 8 KO). (**C**) Quantification of synaptosome preparations from hippocampal tissue shows significant decrease in GluA1 and GluN1 in heterozygous mice. (*P<0.05 for synaptosome lysates n = 8WT, 8HET, 8KO).

Table 1

Statistical Analysis Details

Social Interaction Test				
N	**Test**	**Data**	**Variables**	**Statistical Test (significant data in bold)**
N = 20 WT, 20 HET, 15 KO	3-Box Social Interaction	Trial 1: Base-Line Fig. 2A	Sex, Genotype, & Chamber Posthoc Scheffe contrast of means (Chamber)	3-way rmANOVA; Main effect of Sex: F(1,129) = 0.00118, P = 0.972; Main effect of Genotype: F(2,129) = 0.00112, P = 0.998; **Main effect of Chamber: F(1,129) = 7.37, P < 0.00093**; Main effect of Sex × Genotype Interaction: F(2,129) = 0.00137, P = 0.998; Main effect of Genotype × Chamber: F(4,129) = 1.59, P = 0.180; Main effect of Sex × Chamber: F(2,129) 5 0.028, P = 0.9719; Main effect of Sex × Genotype × Chamber: F(4,129) = 0.213, P = 0.9304
			Back vs. Front	P = 0.447
			Back vs. Middle	**P < 0.00112**
			Front vs. Middle	**P < 0.046**
		Trial 2: Social Preference Fig. 2B	Sex, Genotype, & Interaction Time	3-way rmANOVA; Main effect of Sex: F(1,129) = 0.557, P = 0.457; Main effect of Genotype: F(2,129) = 1.149, P = 0.286; **Main effect of Chamber: F(1,129) = 13.74, P < 0.00036**; Main effect of Sex × Genotype Interaction: F(2,129) = 0.289, P = 0.591; Main effect of Genotype × Chamber: F(4,129) =0.0026, P = 0.959; Main effect of Sex × Chamber: F(2,129) = 1.003, P = 0.319; Main effect of Sex × Genotype × Chamber: F(4,129) = 0.894, P = 0.346
			Interaction zone (Social Time vs. Inanimate Time) within each Genotype	Planned comparisons: **WT: P < 0.010**, HET: P = 0.575, **KO: P < 0.0091**
		Trial 3: Social Novelty Fig. 2C	Sex, Genotype, & Interaction Target	3-way rmANOVA; Main effect of Sex: F(1,129) = 0.802, P = 0.3727; Main effect of Genotype: F(2,129) = 1.18, P = 0.311; Main effect of Target: F(1,129) = 0.801, P < 0.00009; Main effect of Sex × Genotype Interaction: F(2,129) = 1.344, P = 0.266; Main effect of Genotype × Target: F(4,129) = 1.94, P = 0.149; Main effect of Sex × Target: F(2,129) = 0.163, P = 0.686; Main effect of Sex × Genotype × Target: F(4,129) = 0.555, P = 0.575
			Interaction zone (Novel vs. Familiar) within each Genotype	Planned comparisons: **WT: P < 0.016**, HET: P = 0.768, KO: P = 0.352
N = 20 WT, 20 HET, 15 KO	Caged Conspecific	Interaction w/caged mouse Fig 2D	Sex & Genotype Planned Comparison	2-way ANOVA; Main effect of Sex: F(1,54) = 1.48, P = 0.228; Main effect of Genotype: F(2,54) = 2.03, P = 0.14; Sex × Genotype Interaction: F(2,54) = 2.69, P = 0.077
			WT vs. HET	P = 0.686
			WT vs. KO	**P < 0.0066**
			HET vs. KO	**P < 0.042**
N = 10 WT, 10 HET, 7 KO (All Pairs)	Genotype-Sex match	Duration of total interac-tion 2E	Sex & Genotype Posthoc Scheffe contrast of means	2-way ANOVA; Main effect of Sex: F(1,55) = 1.23, P = 0.272; **Main effect of Genotype: F(2,55) = 8.073, P < 0.0009**; Sex × Genotype Interaction: F(2,55) = 0.325, P = 0.723

Social Interaction Test

N	Test	Data	Variables	Statistical Test (significant data in bold)
			WT vs. HET	P = 0.99
			WT vs. KO	**P < 0.003**
			HET vs. KO	**P < 0.005**
		Number of Interaction bouts 2F	Sex & Genotype	2-way ANOVA; **Main effect of Sex: F(1,55) = 12.54, P < 0.0008; Main effect of Genotype: F(2,55) = 25.69, P < 2.1–08**; Sex × Genotype Interaction: F(2,55) = 3.08, P = 0.054
			Posthoc Scheffe contrast of means (genotype)	
			WT vs. HET	P = 0.062
			WT vs. KO	**P < 2.09–08**
			HET vs. KO	**P < 0.0004**
			Posthoc Scheffe contrast of means (sex)	
			WT Male vs. Female	**P < 0.00079**
			HET Male vs. Female	P = 0.919
			KO Male vs. Female	**P < 0.017**
			Posthoc Scheffe contrast of means (female)	
			WT vs. HET	**P < 0.0048**
			WT vs. KO	**P < 0.00001**
			HET vs. KO	P = 0.205
			WT/HET/KO Mean/SEM	27/1.01, 19/2.01, 14.8/1.46
			Posthoc Scheffe contrast of means (Male)	
			WT vs. HET	P = 0.999
			WT vs. KO	**P < 0.00028**
			HET vs. KO	**P < 0.00013**
			WT/HET/KO Mean/SEM	19.2/1.33, 19.25/1.56, 9.4/2.08
N = 20 WT, 20 HET, 15 KO	Social Interaction w/Juvenile	Social Interaction Fig. 2G	Sex, Genotype, & Trial	3-way rmANOVA; Main effect of Sex: F(1,88) =0.056, P = 0.812; Main effect of Genotype: F(2,88) = 0.198, P = 0.820; Main effect of Trial: F(1,88) = 3.587, P = 0.061; Main effect of Sex × Genotype Interaction: F(2,88) = 1.37, P = 0.259; **Main effect of Genotype × Trial: F(2,88) = 3.74, P < 0.027**; Main effect of Sex × Trial: F(1,88) = 0.115, P = 0.735; Main effect of Sex × Genotype × Trial: F(2,88) = 1.175, P = 0.313
			Trial (Initial Test Interaction time vs. Recognition Test Interaction time) within each Genotype	Planned comparisons: **WT: P < 0.000523**, HET: P = 0.901, KO: 0.974.

Repetitive Behavior Test

N	Test	Data Analyzed	Variables	Statistic Test
N = 20 WT, 20 HET, 15 KO	**Grooming**	Time Spent Grooming (sec) Fig. 3A	Sex and Genotype	2-way ANOVA; **Main effect of Sex: F(1,53) =21.50, P < 0.04; Main effect of Genotype: F(2,53) = 88.40, P < 0.011**; Main effect of Sex × Genotype

Social Interaction Test				
N	**Test**	**Data**	**Variables**	**Statistical Test (significant data in bold)**
				Interaction: F(2,53) = 0.295, P = 0.E+0
			Planned Comparison	
			WT vs. KO	**P < 1.21E-08**
			WT vs. HET	**P < 0.0008**
			HET vs. KO Posthoc Scheffe Contrast of means (sex)	P = 0.136
			WT Male vs Female	P = 0.398
			HET Male vs Female	**P < 0.0454**
			KO Male vs Female	P = 0.162
			Posthoc Scheffe Contrast of means (sex) Female	
			WT vs HET	**P < 0.0264**
			WT vs KO	**P < 0.00017**
			HET vs KO	P < 0.2976
			WT/HET/KO Mean/SEM Posthoc Scheffe Contrast of means (sex) Male	71.27/10.8, 140.5/21.24, 180.55/20.34
			WT vs HET	**P < 0.00077**
			WT vs KO	**P < 0.00001**
			HET vs KO	P < 0.7714
			WT/HET/KO Mean/SEM	91.1/14.7, 195.99/21.63, 214.59/17.03

Anxiety and Motor Behavior Test				
N	Test	Data Analyzed	Variables	Statistical Test
N = 20 WT, 20 HET, 15 KO	Open field	Time in center Fig. 3B	Sex and Genotype	2-way ANOVA; Main effect of Sex: F(1,54) = 0.189, P = 0.66; Main effect of Genotype: F(2,54) = 1.35, P = 0.266; Sex × Genotype Interaction: F(2,54) = 0.198, P = 0.82
		Total Distance Traveled Fig. 3C	Sex and Genotype	2-way ANOVA; Main effect of Sex: F(1,54) = 0.3.76, P = 0.19; Main effect of Genotype: F(2,54) = 8.41, P = 0.10; Main effect of Sex × Genotype Interaction: F(2,54) = 0.20, P = 0.09
		Latency to enter light chamber Fig. 3D	Sex and Genotype	2-way ANOVA; Main effect of Sex: F(1,54) = 2.40, P = 0.127; Main effect of Genotype: F(2,54) = 0.109, P = 0.896; Sex × Genotype Interaction: F(2,54) = 0.56, P = 0.56
N = 20 WT, 20 HET, 15 KO	Dark/Light	Time in Light & Dark Chambers Fig. 3E	Sex and Genotype	2-way ANOVA; **Main effect of Sex: F(1,54) = 4.84, P < 0.032**; Main effect of Genotype: F(2,54) = 1.549, P50.222; Sex × Genotype Interaction: F(1,52) = 1.70, P = 0.192
		Time in light chamber	Posthoc Scheffe contrast of means (sex)	
			WT Male vs. Female	P = 0.168
			HET Male vs. Female	P = 0.903
			KO Male vs. Female	**P < 0.015**
			KO Mean/SEM	Male:21.35/12.81 Femlae: 110.37/46.8

Social Interaction Test				
N	**Test**	**Data**	**Variables**	**Statistical Test (significant data in bold)**
			Posthoc Scheffe contrast of means (sex):	
			Female: WT vs. Het	P = 0.174
			WT vs. KO	P = 0.864
			Het vs. KO	P = 0.070
			Male: WT vs. Het	P = 0.910
			WT vs. KO	P = 0.844
			Het vs. KO	P = 0.996
		Time in dark chamber	Sex and Genotype	2-way ANOVA; **Main effect of Sex: F(1,54) = 4.84, P < 0.03**; Main effect of Genotype: F(2,54) = 1.54, P = 0.222; Sex × Genotype Interaction: F(2,54) = 0.1.70, P = 0.192
			Posthoc Scheffe contrast of means (group):	
			Female: WT vs. Het	P = 0.174
			WT vs. KO	P = 0.864
			Het vs. KO	P = 0.070
			Male: WT vs. Het	P = 0.910
			WT vs. KO	P = 0.844
			Het vs. KO	P = 0.996 Posthoc Scheffe contrast of means (sex):
			WT Male vs. Female	P = 0.168
			HET Male vs. Female	P = 0.903
			KO Male vs. Female	**P < 0.015**
			KO Mean/SEM	Male:578.65/12.81 Femlae: 489.62/46.82
N = 20 WT, 20 HET, 15 KO	Elevated Plus Maze	Duration in Closed arms (%) Fig. 3F	Sex and Genotype	2-way ANOVA; Main effect of Sex: F(1,54) = 1.48, P = 0.228; Main effect of Genotype: F(2,54) = 2.03, P = 0.14; Sex × Genotype Interaction: F(2,54) = 2.69, P = 0.077
		Duration in Open arms (%) Fig. 3F	Sex and Genotype	2-way ANOVA; Main effect of Sex: F(1,54) = 0.0042, P = 0.948; Main effect of Genotype: F(2,54) = 3.15, P = 0.051; Sex × Genotype Interaction: F(2,54) = 1.43, P = 0.24
			Planned comparison	
			WT vs. Het	**P < 0.026**
			Het vs. KO	P = 0.708
			WT vs. KO	P = 0.063
N = 20 WT, 20 HET, 15 KO	Rearing	Beam Breaks Fig. 3G	Sex, Genotype, & Bin	3-way rmANOVA; **Main effect of Sex: F(1,659) = 48.88, P < 7.412E-12; Main effect of Genotype: F(2, 659) = 30.59, P < 2.29E-13; Main effect of Bin: F(11,659) = 25.09, P < 0.000001; Main effect of Sex × Genotype Interaction: F(2,659) = 4.72, P < 0.00925**; Main effect of Sex × Bin Interaction: F(11,659) = 0.674, P = 0.763; **Main**

Social Interaction Test				
N	**Test**	**Data**	**Variables**	**Statistical Test (significant data in bold)**
				effect of Genotype × Bin Interaction: F(22,659) = 2.039, P < 0.003; Main effect of Sex × Genotype × Bin Interaction: F(22,659) = 0.431, P = 0.989
			Posthoc Scheffe contrast of means (genotype)	
			WT vs. HET	**P < 1.814E-5**
			WT vs. KO	**P < 4.21E-13**
			HET vs. KO	P = 0.052
			Posthoc Scheffe contrast of means (Sex: Male)	
			WT vs. HET	P = 0.846
			WT vs. KO	P = 0.999
			HET vs. KO	P = 0.802
			Posthoc Scheffe contrast of means (Sex: Female)	
			WT vs. HET	**P < 0.047**
			WT vs. KO	**P < 0.016**
			HET vs. KO	P = 0.957
			Posthoc Scheffe contrast of means (sex):	
			WT Male vs. Female	**P < 0.00064**
			HET Male vs. Female	P = 0.921
			KO Male vs. Female	P = 0.604
		Total Beam Breaks Fig. 3H	Sex and Genotype	2-way ANOVA; **Main effect of Sex: F(1,54) = 7.28, P < 0.0095; Main effect of Genotype: F(2,54) = 4.556, P < 0.0153**; Sex × Genotype Interaction: F(2,54) = 0.703, P = 0.500
			Posthoc Scheffe contrast of means (genotype)	
			WT vs. HET	P = 0.201
			WT vs. KO	**P < 0.016**
			HET vs. KO Posthoc Scheffe contrast of means (Sex: Male)	P = 0.646
			WT vs. HET	P = 0.887
			WT vs. KO	P = 0.475
			HET vs. KO Posthoc Scheffe contrast of means (Sex: Female)	P = 0.830
			WT vs. HET	P = 0.105
			WT vs. KO	**P < 0.023**
			HET vs. KO Posthoc Scheffe contrast of means (sex):	P = 0.852
			WT Male vs. Female	**P < 0.0099**
			HET Male vs. Female	P = 0.433

Social Interaction Test				
N	**Test**	**Data**	**Variables**	**Statistical Test (significant data in bold)**
			KO Male vs. Female Posthoc Scheffe contrast of means (Sex: Male)	P = 0.344
			WT vs. HET	P = 0.105
			WT vs. KO	**P < 0.023**
			HET vs. KO Posthoc Scheffe contrast of means (Sex: Female)	P = 0.852
			WT vs. HET	P = 0.887
			WT vs. KO	P = 0.475
			HET vs. KO	P = 0.830
N = 20 WT, 20 HET, 15 KO	Marbles burying	Marbles buried Fig. 3I	Sex and Genotype	2-way ANOVA; Main effect of Sex: F(1,54) = 0.772, P = 0.384; **Main effect of Genotype: F(2,54) = 21.60, P < 0.00001**; Sex × Genotype Interaction: F(2,54) = 0.333, P = 0.718
			Posthoc Scheffe contrast of means (genotype):	
			WT vs. Het	P = 0.301
			WT vs. KO	**P < 3.57E-07**
			Het vs. KO	**P < 0.00037**
N = 20 WT, 20 HET, 15 KO	Locomotor	Beam Breaks Fig. 3J	Sex and Genotype	3-way rmANOVA; **Main effect of Sex: F(1,54) = 8.66, P < 0.0033**; Main effect of Genotype: F(2,54) = 12.81, **P < 3.1E-06; Main effect of Bin: F(23,1008) = 65.69, P < 0.000001; Main effect of Sex × Genotype Interaction: F(2,54) = 10.30, P < 0.00004;** Main effect of Sex × Bin Interaction: F(23,1008) = 1.17, P = 0.261; Main effect of Genotype × Bin Interaction: F(46,1008)50.959, P = 0.550; Main effect of Sex × Genotype × Bin Interaction: F(46,1008) = 0.49, P = 0.99
			Posthoc Scheffe contrast of means (genotype):	
			WT vs. Het	P = 0.301
			WT vs. KO	**P < 3.57E-07**
			KO Het vs. KO Posthoc Scheffe contrast of means (Sex: Male)	**P < 0.00037**
			WT vs. HET	P = 0.432
			WT vs. KO	P = 0.726
			HET vs. KO Posthoc Scheffe contrast of means (Sex: Female)	P = 0.849
			WT vs. HET	P = 0.989
			WT vs. KO	P = 0.914
			HET vs. KO Posthoc Scheffe contrast of means (sex):	P = 0.967
			WT Male vs. Female	P = 0.122

Social Interaction Test				
N	**Test**	**Data**	**Variables**	**Statistical Test (significant data in bold)**
			HET Male vs. Female	P = 0.939
			KO Male vs. Female	P = 0.697
		Total Beam Breaks Fig. 3K	Sex and Genotype	2-way ANOVA; Main effect of Sex: F(1,47) = 1.02, P = 0.318; Main effect of Genotype: F(2,47) = 1.50, P = 0.232; Sex × Genotype Interaction: F(2,47) = 1.213, P = 0.307
N = 20 WT, 20 HET, 15 KO	Rotarod	Latency to Fall Fig. 3L	Sex, Genotype, and Trial	3-way rmANOVA; **Main effect of Sex: F(1,52) = 19.46, P < 0.00001; Main effect of Genotype: F(2,52) = 14.47, P < 8.57E-07; Main effect of Trial: F(7,408) = 9.986, P < 0.1.70E-11; Main effect of Sex × Genotype Interaction: F(2,52) 518.99, P < 1.33E-08; Main effect of Sex × Trial Interaction: F(7,408) = 5.05, P < 0.00002; Main effect of Genotype × Trial Interaction: F(14,408) = 3.511, P < 0.00002, Main effect of Sex × Genotype × Trial Interaction: F(14,408) = 3.197, P < 0.00008**
			Posthoc Scheffe contrast of means (genotype)	
			WT vs. HET	P = 0.608
			WT vs. KO	**P < 0.00016**
			HET vs. KO	**P < 0.00001**
			Posthoc Scheffe contrast of means (Sex: Female)	
			WT vs. HET	P = 0.385
			WT vs. KO	**P < 0.003**
			HET vs. KO	P = 0.180
			Posthoc Scheffe contrast of means (Sex: Male)	
			WT vs. HET	**P < 1.79E-07**
			WT vs. KO	P = 0.903
			HET vs. KO	**P < 8.31E-07**
			Posthoc Scheffe contrast of means (sex):	
			WT Male vs. Female	**P < 0.0022**
			HET Male vs. Female	**P < 0.00007**
			KO Male vs. Female	P = 0.397
N = 20 WT, 20 HET, 15 KO	Startle	Avg Startle Amplitude Fig. 1M	Sex, Genotype, and dB	3-way rmANOVA; **Main effect of Sex: F(1,259) = 7.98, P < 0.0051; Main effect of Genotype: F(2,259) = 14.47, P < 0.0388; Main effect of dB: F(8, 259) = 75.15, P < 0.00001**; Main effect of Sex × Genotype Interaction: F(2,259) = 0.855, P = 0.426; Main effect of Sex × dB Interaction: F(4,259) = 1.61, P = 0.172; Main effect of Genotype × dB Interaction: F(8,259) = 1.019, P = 0.429, Main effect of Sex × Genotype × Trial Interaction: F(8,259) = 0.158, P = 0.995
N = 20 WT, 20 HET, 15 KO	Prepulse Inhibition	% Inhibition Fig. 3N	Sex, Genotype, and dB	3-way rmANOVA; Main effect of Sex: F(1,143) = 0.254, P = 0.614; Main effect of Genotype: F(2,143) = 0.102, P = 0.902; **Main effect of dB: F(2,**

Social Interaction Test				
N	**Test**	**Data**	**Variables**	**Statistical Test (significant data in bold)**
				143) = 48.48, P < 2.22E-16; Main effect of Sex × Genotype Interaction: F(2,143) = 0.831, P = 0.437; Main effect of Sex × dB Interaction: F(4,143) = 0.038, P = 0.961; Main effect of Genotype × dB Interaction: F(4,143) = 0.667, P = 0.616, Main effect of Sex × Genotype × Trial Interaction: F(4,143) = 0.245, P = 0.912
N = 20 WT, 20 HET, 15 KO	Morris Water Maze	Latency to Platform Fig. 4A	Sex, Genotype, and Day	3-way rmANOVA; Main effect of Sex: F(1,363)51.812, P50.179; **Main effect of Genotype: F(2,363) = 27.07, P < 1.350E-11; Main effect of Day: F(6,363) =7.659, P < 1.053E–7**; Main effect of Sex × Genotype Interaction: F(2,363) = 1.239, P = 0.290; Main effect of Sex × Day Interaction: F(6,363) = 1.05, P = 0.387; **Main effect of Genotype × Day Interaction: F(12,363) = 2.11, P < 0.042**; Main effect of Sex × Genotype × Day Interaction: F(12,363) = 0.818, P = 0.631
			Posthoc Scheffe contrast of means (Genotype)	
			WT vs. HET	P = 0.191
			WT vs. KO	**P < 3.701–11**
			HET vs. KO	**P < 1.547–5**
		Total Distanced Traveled Fig. 4B	Sex, Genotype, and Day	3-way rmANOVA; **Main effect of Sex: F(1,363) = 8.375, P < 0.004; Main effect of Genotype: F(2,363) = 18.78, P < 1.914e-8; Main effect of Day: F(6,363) = 19.45, P < 0.00001; Main effect of Sex × Genotype Interaction: F(2,363) = 4.87, P < 0.008**; Main effect of Sex × Day Interaction: F(6,363) = 0.984, P = 0.435; **Main effect of Genotype × Day Interaction: F(12,363) = 3.036, P < 0.0004**; Main effect of Sex × Genotype × Day Interaction: F(12,363) = 0.808, P = 0.649
			Posthoc Scheffe contrast of means (Genotype)	
			WT vs. HET	P = 0.095
			WT vs. KO	**P < 2.16e-8**
			HET vs. KO	**P < 0.003**
			Posthoc Scheffe contrast of means (Sex: Male)	
			WT vs. HET	P = 0.789
			WT vs. KO	P = 0.464
			HET vs. KO	P = 0.908
			Posthoc Scheffe contrast of means (Sex: Female)	
			WT vs. HET	P = 0.635
			WT vs. KO	P = 0.124
			HET vs. KO	P = 0.628
			Posthoc Scheffe contrast	

Social Interaction Test				
N	**Test**	**Data**	**Variables**	**Statistical Test (significant data in bold)**
			of means (sex):	
			WT Male vs. Female	P = 0.732
		Percent Thigmotaxis Fig. 4C	HET Male vs. Female	P = 0.577
			KO Male vs. Female	P = 0.217
			Sex, Genotype, and Day	3-way rmANOVA; **Main effect of Sex: F(1,363) = 4.05, P < 0.044; Main effect of Genotype: F(2,363) = 44.96, P < 0.00001; Main effect of Day: F(6,363) = 11.07, P < 3.08e–7**; Main effect of Sex × Genotype Interaction: F(2,363) = 1.133, P = 0.323; Main effect of Sex = Day Interaction: F(6,363) = 0.378, P = 0.892; **Main effect of Genotype × Day Interaction: F(12,363) × 2.088, P < 0.017**; Main effect of Sex × Genotype × Day Interaction: F(12,363) = 0.394, P = 0.965
		Probe Trial Fig. 4D	Posthoc Scheffe contrast of means (Sex: Male)	
			WT vs. HET	P = 0.175
			WT vs. KO	**P < 1.11e016**
			HET vs. KO	**P < 0.00001**
			Sex, Genotype, and Quadrant	3-way rmANOVA; Main effect of Sex: F(1,207) = 2.78e-5, P = 0.995; **Main effect of Genotype: F(2,207) = 3.05e-5, P = 0.99; Main effect of Quadrant: F(3,207) = 19.28, P < 6.43e-11**; Main effect of Sex × Genotype Interaction: F(2,207) = 5.01e-6, P = 0.999; Main effect of Sex × Quadrant Interaction: F(3,207) = 1.469, P = 0.224; **Main effect of Genotype × Quadrant Interaction: F(6,207) = 2.623, P < 0.01**; Main effect of Sex × Genotype × Quadrant Interaction: F(6, 207) =0.523, P = 0.789
			Planned comparison (WT)	
			Target vs. Near	**P < 2.01e-9**
			Target vs. Far	**P < 0.0001**
			Target vs. Opposite (HET)	**P < 2.02e–7**
			Target vs. Near	**P < 0.0001**
			Target vs. Far	**P < 0.0074**
			Target vs. Opposite (KO)	**P < 0.001**
			Target vs. Near	P = 0.105
			Target vs. Far	P = 0.618
			Target vs. Opposite	P = 0.476